

# Second-order perturbation theory: the problem of infinite mode coupling

Jeremy Miller,<sup>1</sup> Barry Wardell,<sup>2,3</sup> and Adam Pound<sup>1</sup>

<sup>1</sup>*Mathematical Sciences and STAG Research Centre,  
University of Southampton, Southampton, SO17 1BJ, United Kingdom*  
<sup>2</sup>*School of Mathematical Sciences and Complex & Adaptive Systems Laboratory,  
University College Dublin, Belfield, Dublin 4, Ireland*  
<sup>3</sup>*Department of Astronomy, Cornell University, Ithaca, NY 14853, USA*

(Dated: September 24, 2018)

Second-order self-force computations, which will be essential in modeling extreme-mass-ratio inspirals, involve two major new difficulties that were not present at first order. One is the problem of large scales, discussed in [Phys. Rev. D 92, 104047 (2015)]. Here we discuss the second difficulty, which occurs instead on small scales: if we expand the field equations in spherical harmonics, then because the first-order field contains a singularity, we require an arbitrarily large number of first-order modes to accurately compute even a single second-order mode. This is a generic feature of nonlinear field equations containing singularities, allowing us to study it in the simple context of a scalar toy model in flat space. Using that model, we illustrate the problem and demonstrate a robust strategy for overcoming it.

## I. INTRODUCTION AND SUMMARY

Gravitational self-force theory [1–3] has proven to be an important tool in efforts to model compact binary inspirals. It is currently the only viable method of accurately modeling extreme-mass-ratio inspirals (EMRIs) [4, 5], it is a potentially powerful means of modeling intermediate-mass-ratio inspirals, and by interfacing with other methods, it can even be used to validate and improve models of comparable-mass binaries [6–11]. However, the self-force model is based on an asymptotic expansion in the limit  $m/M \rightarrow 0$ , where  $m$  and  $M$  are the two masses in the system. The model’s accuracy is hence limited by the perturbative order at which it is truncated. Unfortunately, although numerous concrete self-force computations of binary dynamics have been performed (see the reviews [1, 4, 12] and Refs. [13–19] for some more recent examples), until now they have been restricted to first perturbative order, limiting their capacity to assist other models and rendering them insufficiently accurate to model EMRIs [20].

In recent years, substantial effort has gone into overcoming this limitation [2, 21–30]. The foundations of second-order self-force theory are now established [2, 24–26], the key analytical ingredients are in place [27], and at least in some scenarios, practical formulations of the second-order field equations have been developed [30–32]. However, concrete solutions to the field equations have remained elusive.

There have been two major obstacles to finding these solutions. The first is the problem of large scales, described in Ref. [29], which manifests in spurious unbounded growth and ill-defined retarded integrals. As demonstrated in a simple toy model in Ref. [29], this obstacle can be overcome by utilizing multiscale and matched-expansion techniques; full descriptions of these techniques in the gravitational problem will be given in future papers. The second major obstacle arises in the opposite extreme: rather than a problem on large scales,

it is a problem on small ones.

To introduce the problem, we refer to the Einstein equations through second order, which we can write as

$$\delta G_{\mu\nu}[h^1] = 8\pi T_{\mu\nu}, \quad (1)$$

$$\delta G_{\mu\nu}[h^2] = -\delta^2 G_{\mu\nu}[h^1, h^1]. \quad (2)$$

Here the metric has been expanded as  $g_{\mu\nu} + (m/M)h_{\mu\nu}^1 + (m/M)^2 h_{\mu\nu}^2 + \mathcal{O}(m^3)$ ;  $T_{\mu\nu}$  is the stress-energy of a point particle, representing the leading approximation to the smaller object  $m$  on the background  $g_{\mu\nu}$ ;  $\delta G_{\mu\nu}$  is the linearized Einstein tensor (in some appropriate gauge [28]); and  $\delta^2 G_{\mu\nu}[h^1, h^1]$  is the second-order Einstein tensor, which has the schematic form  $h^1 \partial^2 h^1 + \partial h^1 \partial h^1$ . Because  $h_{\mu\nu}^1$  is singular at the particle, Eq. (2) is only valid at points away from the particle’s worldline [26], but that suffices for our purposes here.

Equations (1)–(2) can in principle be solved in four dimensions (4D). However, in practice it is desirable to reduce their dimension by decomposing them into a basis of harmonics. For illustration let us use some basis of tensor harmonics  $Y_{\mu\nu}^{ilm}$ ; here we use the notation of Barack-Lousto-Sago [33, 34], with  $i = 1, \dots, 10$ , but the particular choice of basis, whether spherical or spheroidal (for example), is immaterial. We have

$$h_{\mu\nu}^n = \sum_{ilm} h_{ilm}^n Y_{\mu\nu}^{ilm} \quad (3)$$

and

$$\delta G_{ilm}[h^1] = 8\pi T_{ilm}, \quad (4)$$

$$\delta G_{ilm}[h^2] = -\delta^2 G_{ilm}[h^1, h^1]. \quad (5)$$

Now consider the source term  $\delta^2 G_{ilm}$ . Substituting the expansion (3) into  $\delta^2 G_{\mu\nu}$  leads to a mode-coupling formula with the schematic form

$$\delta^2 G_{ilm} = \sum_{\substack{i_1 l_1 m_1 \\ i_2 l_2 m_2}} \mathcal{D}_{ilm}^{i_1 l_1 m_1 i_2 l_2 m_2} [h_{i_1 l_1 m_1}^1, h_{i_2 l_2 m_2}^1], \quad (6)$$

where  $\mathcal{D}_{ilm}^{i_1 l_1 m_1 i_2 l_2 m_2}$  is a bilinear differential operator (given explicitly in Ref. [30]). A single mode  $\delta^2 G_{ilm}$  is an infinite sum over first-order modes  $h_{ilm}^1$ . If  $h_{ilm}^1$  falls off sufficiently rapidly with  $l$ , then the summation poses no problem. However, if  $h_{ilm}^1$  falls off slowly with  $l$ , then the summation is potentially intractable. This is precisely the situation near the point-particle singularity in Eq. (4).  $h_{\mu\nu}^1$  behaves approximately as a Coulomb field, blowing up as  $\sim 1/\rho$ , where  $\rho$  is a spatial distance from the particle. The individual modes  $h_{ilm}^1 Y_{\mu\nu}^{ilm}$ , after summing over  $m$ , then go as  $\sim l^0$  on the particle [4, 32], not decaying at all; at points *near* the particle, the decay is arbitrarily slow.

This behavior can be understood from the textbook example of a Coulomb field  $\varphi$  in flat space. For a static charged particle at radius  $r_0$ , the field's modes behave as  $\varphi_{lm} Y_{lm} \sim (r_{<}/r_{>})^l$ , where  $r_{<} := \min(r_0, r)$  and  $r_{>} := \max(r_0, r)$ . On the particle, where  $r = r_0$ , we have  $\varphi_{lm} Y_{lm} \sim l^0$ . At any point  $r \neq r_0$ , we have exponential decay with  $l$ , but that decay is arbitrarily slow when  $r \approx r_0$ . Extrapolating this behavior to the gravitational case (6), we can infer that unless the coupling operator  $\mathcal{D}_{ilm}^{i_1 l_1 m_1 i_2 l_2 m_2}$  introduces rapid decay (which it does not), we are faced with the following tenuous position: *to obtain a single mode of the second-order source near the particle, we must sum over an arbitrarily large number of first-order modes.*

In this paper, we explicate this problem and present a robust, broadly applicable method of surmounting it. Rather than facing the challenge head-on in gravity, we retreat to the same flat-space scalar toy model as was used in Ref. [29]. In place of the gravitational field equations (4)–(5), we consider the field equations

$$\square\varphi_1 = -4\pi\varrho, \quad (7)$$

$$\square\varphi_2 = t^{\alpha\beta}\partial_\alpha\varphi_1\partial_\beta\varphi_1 =: S. \quad (8)$$

Here, in Cartesian coordinates  $(t, x^i)$ ,  $\square = -\partial_t^2 + \partial^i\partial_i$  is the flat-space d'Alembertian,

$$\varrho := \frac{\delta(x^i - x_p^i)}{dt/d\tau} \quad (9)$$

is a point charge distribution moving on a worldline  $x_p^\mu(t) = (t, x^i(t))$  with proper time  $\tau$ , and  $t^{\mu\nu} := \text{diag}(1, 1, 1, 1)$ . With our chosen source terms, the first-order field  $\varphi_1$  mimics the behavior of  $h_{\mu\nu}^1$ , and the second-order source  $S$  mimics the behavior of  $\delta^2 G_{ilm}$ .

Like Eq. (5), Eq. (8) is well defined only at points off the worldline. To solve it globally, one would have to rewrite it as  $\square\varphi_2^{\mathcal{R}} = S - \square\varphi_2^{\mathcal{P}}$  [29], where  $\varphi_2^{\mathcal{P}}$  is an analytically determined, singular ‘‘puncture’’ that guarantees the total field has the correct physical behavior near the particle, and  $\varphi_2^{\mathcal{R}} := \varphi_2 - \varphi_2^{\mathcal{P}}$  is the regular ‘‘residual’’ difference between the total field and the puncture. However, here we only wish to address the preliminary question: *given the spherical harmonic modes of  $\varphi_1$ , how can we accurately compute the modes of  $S$ ?* Once that question is answered, the same method can be carried over

directly to the gravitational case to compute the source  $\delta^2 G_{ilm}$ , and Eq. (5) can then be solved via a puncture scheme of the sort described in Refs. [31, 32] (see also Ref. [29]).

Before describing the technical details of our computations, we summarize the problem, our strategy for overcoming it, and our successful application of that strategy. For simplicity, we fix the particle on a circular orbit of radius  $r_0$ . The modes  $\varphi_{lm}^{\text{ret}}$  of the first-order retarded field are then easily found; they are given by Eqs. (17) and (18). (To streamline the notation, we shall omit the subscript 1 on first-order fields.) From those modes, one can naively attempt to compute the modes  $S_{lm}$  of the source using an analog of Eq. (6), given explicitly by Eq. (31) below. Figure 1 shows the failure of this direct computation in the case of the monopole mode  $S_{00}$ . The higher the curve in the figure, the greater the number of first-order modes included in the sum, up to a maximum  $l = l_{\text{max}}$ . Although the convergence is rapid at points far from the particle, it becomes arbitrarily slow near the particle's radial position  $r_0$ . In principle, this obstacle could be overcome with brute force, simply adding more modes until we achieve some desired accuracy at some desired nearest point to the particle. However, that relies on having all the modes of the retarded field at hand; in most applications of the self-force formalism, the retarded field modes are found numerically, and the number of modes is limited by practical computational demands. Hence, we should rephrase the question from the previous paragraph: given the spherical harmonic modes of  $\varphi_1$  *up to some maximum*  $l = l_{\text{max}}$ , how can we accurately compute the modes of  $S$ ?

Our answer to this question is to utilize a 4D approximation to the point-particle singularity. As is well known, the retarded field of a point particle can be split into two pieces as  $\varphi^{\text{ret}} = \varphi^S + \varphi^R$  [35], where  $\varphi^S$  is the Detweiler-Whiting singular field, which is a particular solution to Eq. (7), and  $\varphi^R$  is the corresponding regular field, which is a smooth solution to  $\square\phi^R = 0$ . The slow falloff of  $\varphi_{lm}^{\text{ret}}$  with  $l$  is entirely isolated in the modes of the singular field,  $\varphi_{lm}^S$ ; because  $\varphi^R$  is smooth, its modes  $\varphi_{lm}^R$  have a uniform exponential falloff with  $l$ . Generally, there is no way to obtain a closed-form expression for  $\varphi^S$ , but we *can* easily obtain a local expansion of  $\varphi^S$  in powers of distance from the particle. A truncation of that expansion at some finite order provides a puncture, of the sort alluded to above, which we denote by  $\varphi^{\mathcal{P}}$ ; it is given explicitly by Eq. (23) below. It defines a residual field  $\varphi^{\mathcal{R}} := \varphi^{\text{ret}} - \varphi^{\mathcal{P}}$  that approximates  $\varphi^R$ . We make use of all this by writing the source in the suggestively quadratic form  $S[\varphi, \varphi]$ , and in some region near the particle, splitting the field into the two pieces  $\varphi^{\mathcal{P}} + \varphi^{\mathcal{R}}$ . An  $lm$  mode of  $S$  can then be written as

$$S_{lm} = S_{lm}[\varphi^{\mathcal{R}}, \varphi^{\mathcal{R}}] + 2S_{lm}[\varphi^{\mathcal{R}}, \varphi^{\mathcal{P}}] + S_{lm}[\varphi^{\mathcal{P}}, \varphi^{\mathcal{P}}]. \quad (10)$$

The first two terms,  $S_{lm}[\varphi^{\mathcal{R}}, \varphi^{\mathcal{R}}]$  and  $S_{lm}[\varphi^{\mathcal{R}}, \varphi^{\mathcal{P}}]$ , can be computed from the modes of  $\varphi^{\mathcal{R}}$  and  $\varphi^{\mathcal{P}}$  using

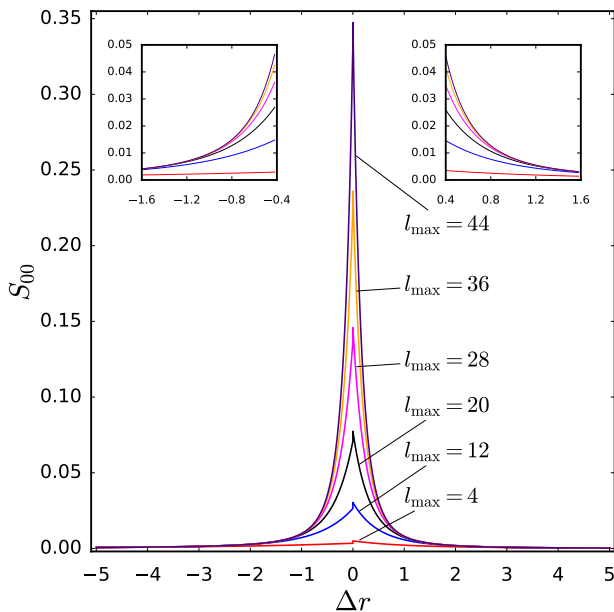


FIG. 1. The source mode  $S_{00}[\varphi^{\text{ret}}, \varphi^{\text{ret}}]$  as a function of  $\Delta r := r - r_0$ , with an orbital radius  $r_0 = 10$ , as computed from the mode-coupling formula (31). To assess the convergence of the sum in Eq. (31), we truncate the first-order field modes  $\varphi_{lm}$  at a maximum  $l$  value  $l_{\text{max}}$ , and we display the behavior of  $S_{00}$  for various values of  $l_{\text{max}}$ . The insets show that far from the particle, the sum converges rapidly with  $l_{\text{max}}$ . However, near the particle there is no evidence of numerical convergence.

Eq. (31); for sufficiently smooth  $\varphi^{\mathcal{R}}$ , the convergence will be sufficiently rapid. The problem of slow convergence is then isolated in the third term,  $S_{lm}[\varphi^{\mathcal{P}}, \varphi^{\mathcal{P}}]$ . This term cannot be accurately computed from the modes of  $\varphi^{\mathcal{P}}$ . However,  $S[\varphi^{\mathcal{P}}, \varphi^{\mathcal{P}}]$  can be computed in 4D using the 4D expression for  $\varphi^{\mathcal{P}}$ . Its modes  $S_{lm}[\varphi^{\mathcal{P}}, \varphi^{\mathcal{P}}]$  can then be computed directly, without utilizing the mode-coupling formula (31), simply by integrating the 4D expression against a scalar harmonic.

Our strategy is hence summarized as follows:

1. compute the modes  $\varphi_{lm}^{\mathcal{P}}$  by direct integration of the 4D expression (40). From the result, and Eqs. (17)–(18), compute the modes  $\varphi_{lm}^{\mathcal{R}} = \varphi_{lm}^{\text{ret}} - \varphi_{lm}^{\mathcal{P}}$
2. evaluate  $S_{lm}[\varphi^{\mathcal{R}}, \varphi^{\mathcal{R}}]$  and  $S_{lm}[\varphi^{\mathcal{R}}, \varphi^{\mathcal{P}}]$  using the mode-coupling formula (31)
3. evaluate  $S[\varphi^{\mathcal{P}}, \varphi^{\mathcal{P}}]$  in 4D, using Eq. (40), and obtain its modes  $S_{lm}[\varphi^{\mathcal{P}}, \varphi^{\mathcal{P}}]$  by direct integration
4. combine these results in Eq. (10).

This strategy is to be applied in some region around  $r = r_0$ ; outside that region, one may simply use the retarded modes in Eq. (31) without difficulty.

Figure 2 displays a successful implementation of this strategy. The true source mode  $S_{00}$ , as computed via our strategy, is shown in thick solid blue. The same mode  $S_{00}$

as computed via mode coupling from  $\varphi_{lm}^{\text{ret}}$ , with a finite  $l_{\text{max}}$ , is shown in thin solid grey. As we can see, the two results agree far from the particle, where the source mode as computed via mode coupling has converged. But near the particle, the results differ by an arbitrarily large amount; the true source correctly diverges at  $r = r_0$ , due to the singularity in the first-order field, while the source computed via mode coupling remains finite due to the truncation at finite  $l_{\text{max}}$ .

In the remaining sections, we describe the technical details of our strategy, as well as the challenges that arise in implementing it. Section II summarizes the various relevant fields—retarded and advanced, singular and regular, puncture and residual. Section III derives the coupling formula that expresses a second-order source mode  $S_{lm}$  as a sum over first-order field modes. Section IV details the computation of  $S_{lm}[\varphi^{\mathcal{R}}, \varphi^{\mathcal{R}}]$  and  $S_{lm}[\varphi^{\mathcal{R}}, \varphi^{\mathcal{P}}]$ ; Sec. V, the computation of  $S_{lm}[\varphi^{\mathcal{P}}, \varphi^{\mathcal{P}}]$ . In Sec. VI, we reiterate the outline of our strategy as it applies to the gravitational case; the successful application to gravity, recently reported in Ref. [36], will be detailed in a future paper.

To avoid repetition, we state in advance that all plots are for a particle at radius  $r_0 = 10$ .

## II. FIRST-ORDER FIELDS

### A. Retarded and advanced solutions

To begin, we work in spherical polar coordinates  $(t, r, \theta^A)$ , where  $\theta^A := (\theta, \phi)$ . We place the particle on the equatorial circular orbit  $x_p^\mu(t) = (t, r_0, \pi/2, \Omega t)$  with normalized four-velocity  $u^\mu = (1 - r_0^2 \Omega^2)^{-1/2} (1, 0, 0, \Omega)$ , and we adopt a Keplerian frequency  $\Omega = \sqrt{1/r_0^3}$ . The point source (9) can then be expanded in spherical and frequency harmonics by rewriting it as

$$\varrho = \frac{\delta(r - r_p)}{r^2 u^t} \sum_{lm} Y_{lm}^*(\theta_p^A) Y_{lm}(\theta^A) \quad (11)$$

and using  $Y_{lm}^*(\theta_p^A) = e^{-im\Omega t} Y_{lm}(\pi/2, 0)$ . Here  $u^t = \frac{dt}{d\tau} = (1 - r_0^2 \Omega^2)^{-1/2}$ .

Most of the fields we are interested in can be constructed by integrating this source against a Green's function. The retarded and advanced Green's functions satisfying  $\square G(x, x') = -4\pi \delta^4(x - x')$  are given by

$$G^{\text{ret/adv}}(x, x') = \frac{\delta(t - t' \mp |\vec{x} - \vec{x}'|)}{|\vec{x} - \vec{x}'|}, \quad (12)$$

where  $\vec{x}$  is a Cartesian three-vector. The Fourier transforms,  $G_\omega^{\text{ret/adv}} = \int e^{i\omega(t-t')} G^{\text{ret/adv}}(x, x') dt$ , are

$$G_\omega^{\text{ret/adv}} = \frac{e^{\pm i\omega|\vec{x} - \vec{x}'|}}{|\vec{x} - \vec{x}'|}, \quad (13)$$

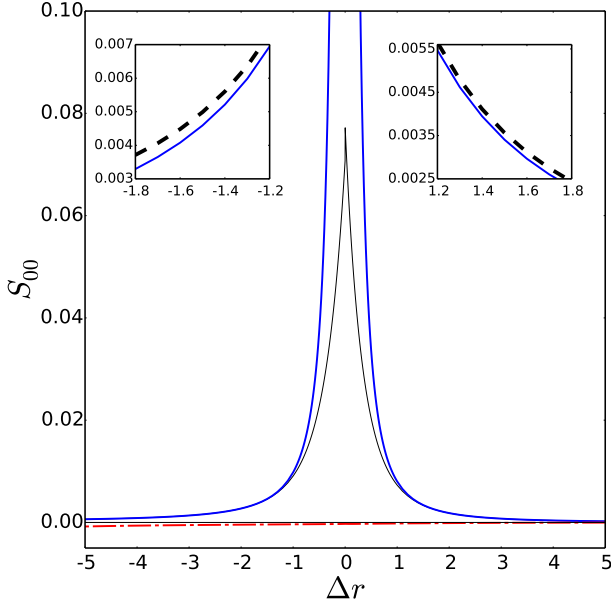


FIG. 2. The source mode  $S_{00}[\varphi^{\text{ret}}, \varphi^{\text{ret}}]$  and its two contributions as functions of  $\Delta r$ , as computed with the strategy outlined in the text. The dot-dashed red curve shows the contribution from  $S_{00}[\varphi^{\text{R}}, \varphi^{\text{R}}] + 2S_{00}[\varphi^{\text{R}}, \varphi^{\text{P}}]$ , the dashed black curve shows the contribution from  $S_{00}[\varphi^{\text{P}}, \varphi^{\text{P}}]$ , and the thick solid blue curve shows their sum  $S_{00}[\varphi^{\text{ret}}, \varphi^{\text{ret}}]$ , which diverges at  $\Delta r = 0$ . On the scale of the main plot,  $S_{00}[\varphi^{\text{R}}, \varphi^{\text{R}}]$  is indistinguishable from  $S_{00}[\varphi^{\text{ret}}, \varphi^{\text{ret}}]$ ; the insets show that they differ by a small, but distinguishable amount, which is made up by  $S_{00}[\varphi^{\text{R}}, \varphi^{\text{R}}] + 2S_{00}[\varphi^{\text{R}}, \varphi^{\text{P}}]$ . For comparison, the thin grey curve displays the result for  $S_{00}[\varphi^{\text{ret}}, \varphi^{\text{ret}}]$  as computed from the mode-coupling formula (31), which agrees with the correct result far from the particle but differs strongly from it near the particle. All curves were generated with  $r_0 = 10$ , all four orders in the puncture (23), and  $l_{\text{max}} = 20$ .

which can be expanded in spherical harmonics as

$$G_{\omega}^{\text{ret/adv}} = \mp i \sum_{lm} \omega j_l(\omega r_{<}) h_l^{(1,2)}(\omega r_{>}) Y_{lm}^*(\theta^{A'}) Y_{lm}(\theta^A). \quad (14)$$

Here the upper sign and  $h_l^{(1)}$  correspond to the retarded solution, and the lower sign and  $h_l^{(2)}$  to the advanced.  $h_l^{(1)}$  and  $h_l^{(2)}$  are the spherical Hankel functions of the first and second kind,  $j_l$  is the spherical Bessel function of the first kind, and when used in the Green's function,  $r_{\leq} := \min/\max(r, r')$ . In the static limit  $\omega \rightarrow 0$ , the retarded and advanced Green's functions both reduce to

$$G^{\text{ret/adv}} = \frac{1}{|\vec{x} - \vec{x}'|} = \sum_{lm} \frac{1}{2l+1} \frac{r_{<}^l}{r_{>}^{l+1}} Y_{lm}^*(\theta^{A'}) Y_{lm}(\theta^A). \quad (15)$$

Integrating against these Green's functions, we find the retarded and advanced solutions

$$\varphi^{\text{ret/adv}} = \sum_{lm} \varphi_{lm}^{\text{ret/adv}}(r) e^{-im\Omega t} Y_{lm}(\theta^A), \quad (16)$$

where

$$\varphi_{lm}^{\text{ret/adv}} = \pm \frac{4\pi i}{u^t} N_{lm} m \Omega j_l(m\Omega r_{<}) h_l^{(1,2)}(m\Omega r_{>}) \quad (17)$$

for  $m \neq 0$ , and

$$\varphi_{l0}^{\text{ret/adv}} = \frac{4\pi}{u^t} \frac{N_{l0}}{2l+1} \frac{r_{<}^l}{r_{>}^{l+1}} \quad (18)$$

for  $m = 0$ . Here  $N_{lm} := Y_{lm}(\pi/2, 0)$ , and we have reverted to the previous notation  $r_{\leq} := \min/\max(r, r_0)$ .

As discussed in the introduction, the large- $l$  behavior of these fields is the source of the infinite-coupling problem. Noting that  $N_{l0} \sim l^0$ , we see that the stationary modes in Eq. (18) behave as  $\varphi_{l0} \sim \frac{1}{l} \frac{r_{<}^l}{r_{>}^{l+1}}$ . Hence,  $\varphi_{l0}$  decays exponentially with  $l$  at points far from  $r = r_0$ , still exponentially but more slowly at points close to  $r = r_0$ , and as  $l^{-1}$  at  $r = r_0$ . The oscillatory,  $m \neq 0$  modes exhibit similar behavior, although it is not obvious from Eq. (17). After summing  $\varphi_{lm} Y_{lm}$  over  $m$ , the large- $l$  behavior becomes  $\sim l^0$  on the particle, with an exponential but arbitrarily weak suppression at points slightly off the particle. The quantitative consequences of this, already displayed in Fig. 1, will be spelled out in later sections.

## B. Singular and regular fields

In flat space, the Detweiler-Whiting singular field is simply  $\varphi^S := \frac{1}{2}(\varphi^{\text{ret}} + \varphi^{\text{adv}})$ . Its four-dimensional form can be written as

$$\varphi^S = \frac{1}{2} \int [G^{\text{ret}}(x, x') + G^{\text{adv}}(x, x')] \varrho(x') d^4 x'. \quad (19)$$

Its modes are more easily found directly from Eqs. (17) and (18). For  $m \neq 0$ ,

$$\varphi_{lm}^S = \frac{4\pi}{u^t} N_{lm} m \Omega j_l(m\Omega r_{<}) y_l(m\Omega r_{>}), \quad (20)$$

where  $y_l$  is the spherical Bessel function of the second kind. For  $m = 0$ ,  $\varphi_{l0}^S = \varphi_{l0}^{\text{ret/adv}}$ .

Correspondingly, in flat space the regular field is  $\varphi^R = \varphi^{\text{ret}} - \varphi^S = \frac{1}{2}(\varphi^{\text{ret}} - \varphi^{\text{adv}})$ . Its four-dimensional form can be written as an integral analogous to (19). Its modes can be found straightforwardly from Eqs. (17) and (18). For  $m \neq 0$ ,

$$\varphi_{lm}^R = \frac{4\pi i}{u^t} N_{lm} m \Omega j_l(m\Omega r_{<}) j_l(m\Omega r_{>}), \quad (21)$$

and for  $m = 0$ ,  $\varphi_{l0}^R = 0$ .

## C. Puncture and residual fields

The puncture field  $\varphi^P$  is obtained in 4D by performing a local expansion of the integral representation (19)

of the singular field. That procedure is common in the literature, and so we do not belabor it here; instead we refer the reader to, e.g., Ref. [37] for details, and give here only the main results. Letting  $\lambda := 1$  count powers

of distance from the particle, the covariant expansion of the flat-space puncture to fourth-from-leading order in distance is

$$\begin{aligned} \varphi^S(x; x_p) = & \frac{1}{\bar{s}} + \frac{\sigma_a(\bar{s}^2 - \bar{r}^2)}{2\bar{s}^3} + \frac{a^2\bar{s}^2(\bar{r}^4 - 6\bar{r}^2\bar{s}^2 - 3\bar{s}^4) + 9\sigma_a^2(\bar{r}^2 - \bar{s}^2)^2 - 4\bar{r}\bar{s}^2\sigma_{\dot{a}}(\bar{r}^2 - 3\bar{s}^2)}{24\bar{s}^5} \\ & + \frac{1}{48\bar{s}^7} \left[ 2\bar{r}\bar{s}^4 a^\alpha \dot{a}_\alpha (\bar{r}^4 - 10\bar{r}^2\bar{s}^2 - 15\bar{s}^4) - 3a^2\bar{s}^2\sigma_a(\bar{r}^6 - 5\bar{r}^4\bar{s}^2 + 15\bar{r}^2\bar{s}^4 + 5\bar{s}^6) \right. \\ & \left. + 4\sigma_a\sigma_{\dot{a}}\bar{r}\bar{s}^2(3\bar{r}^4 - 10\bar{r}^2\bar{s}^2 + 15\bar{s}^4) - 15\sigma_a^3(\bar{r}^2 - \bar{s}^2)^3 - 2\sigma_{\dot{a}}\bar{s}^4(\bar{r}^4 - 6\bar{r}^2\bar{s}^2 - 3\bar{s}^4) \right] + \mathcal{O}(\lambda^3). \end{aligned} \quad (22)$$

where the terms are  $\mathcal{O}(\lambda^{-1})$ ,  $\mathcal{O}(\lambda^0)$ ,  $\mathcal{O}(\lambda^1)$  and  $\mathcal{O}(\lambda^2)$ , respectively. Here, we follow the notation of Ref. [37]: we make use of the compact notation of Haas and Poisson [38],  $\sigma_X := \sigma_\alpha X^\alpha$  for any vector  $X^\alpha$ ; the bi-scalar  $\sigma(x, x_p)$  is the Synge world function, equal to one half of the squared geodesic distance between  $x$  and  $x_p$ , and  $\sigma_\alpha := \frac{\partial\sigma}{\partial x_p^\alpha}$ ; the vectors  $a^\alpha := u^\beta \nabla_\beta u^\alpha$ ,  $\dot{a}^\alpha := u^\beta \nabla_\beta a^\alpha$  and  $\ddot{a}^\alpha := u^\beta \nabla_\beta \dot{a}^\alpha$  are the acceleration and its first and second derivatives, respectively; and the quantities  $\bar{r} := \sigma_\alpha u^\alpha$  and  $\bar{s} := \sqrt{(g^{\alpha\beta} + u^\alpha u^\beta)\sigma_\alpha \sigma_\beta}$  are projected components of the geodesic distance from the field point to the reference point  $x_p$  on the worldline. In our case,  $g_{\alpha\beta}$  is the metric of flat spacetime and  $\nabla_\alpha$  is the covariant derivative compatible with it.

To facilitate the computation of spherical harmonic modes, it is customary to express the field in a rotated coordinate system in which the particle is momentarily at the north pole. We label the angles in this system  $\alpha^{A'} := (\alpha, \beta)$ , such that at a given instant  $t$ , the particle sits at  $\alpha = 0$ . More details can be found in the Appendix. As we describe there and in later sections, in our calculations this rotation introduces new complications and loses some of its traditional advantages. Nevertheless, its benefits outweigh its drawbacks.

In terms of the rotated angles  $\alpha^{A'}$ , a puncture satisfying  $\varphi^P = \varphi^S + \mathcal{O}(\lambda^3)$  can be obtained from a coordinate expansion of Eq. (22). For the circular orbits we are interested in here, this is given explicitly by

$$\varphi^P = \lambda^{-1}\varphi_{(-1)}^P + \lambda^0\varphi_{(0)}^P + \lambda\varphi_{(1)}^P + \lambda^2\varphi_{(2)}^P, \quad (23)$$

where

$$\varphi_{(-1)}^P = \frac{1}{\rho}, \quad (24a)$$

$$\begin{aligned} \varphi_{(0)}^P = & -\frac{\Delta r}{2r_0\rho\chi}(1 - 2v^2s^2) \\ & + \frac{\Delta r^3}{2r_0\chi_0\chi\rho^3}(1 - 2v^2s^2 + v^4s^2), \end{aligned} \quad (24b)$$

$$\varphi_{(1)}^P = \frac{3\Delta r^6}{8r_0^2\rho^5\chi_0^2\chi^2}(1 - 2v^2s^2 + v^4s^2)^2$$

$$\begin{aligned} & + \frac{\rho v^2}{24r_0^2\chi_0^2\chi^2}[3v^6s^2 - 3(1 + s^2) - 3v^2(2 - 7s^2) \\ & + v^4(1 - 5s^2 - 8s^4)] + \frac{\Delta r^2}{24r_0^2\rho\chi_0^2\chi^2}[9 \\ & - 18v^2(1 + s^2) - 6v^8s^2(1 - 4s^2) \\ & + 3v^4(5 + 8s^2 + 8s^4) - 2v^6(1 + 4s^2 + 22s^4)] \\ & + \frac{\Delta r^4}{24r_0^2\rho^3\chi_0^2\chi^2}[-18 + 3v^8s^2(1 - 9s^2) \\ & + 3v^2(7 + 19s^2) - 3v^4(1 + 21s^2 + 20s^4) \\ & + v^6(1 + s^2 + 88s^4)], \end{aligned} \quad (24c)$$

$$\begin{aligned} \varphi_{(2)}^P = & \frac{5\Delta r^9}{16r_0^3\rho^7\chi_0^3\chi^3}(1 - 2v^2s^2 + v^4s^2)^3 \\ & - \frac{\Delta r\rho v^2}{48r_0^3\chi_0^3\chi^3}[6v^{10}s^4 + 3(1 + s^2) \\ & + v^8s^2(7 - 8s^2 - 32s^4) + 3v^2(11 - 14s^2 + 2s^4) \\ & + v^4(13 - 62s^2 + 16s^4) \\ & - v^6(1 + 50s^2 - 124s^4 + 16s^6)] \\ & - \frac{\Delta r^7}{16r_0^3\rho^5\chi_0^3\chi^3}[15 - 3v^{12}s^4(1 - 7s^2) \\ & - 3v^2(6 + 25s^2) + 3v^4(1 + 33s^2 + 46s^4) \\ & - v^{10}s^2(1 - 8s^2 + 112s^4) \\ & + v^8s^2(2 + 65s^2 + 188s^4) \\ & - v^6(1 + 22s^2 + 211s^4 + 96s^6)] \\ & - \frac{\Delta r^3}{48r_0^3\rho\chi_0^3\chi^3}[15 - 3v^{12}s^4(7 - 16s^2) \\ & - 3v^2(16 + 17s^2) - v^{10}s^2(17 - 13s^2 + 128s^4) \\ & + 3v^4(11 + 61s^2 + 14s^4) \\ & - v^6(26 + 158s^2 + 125s^4 + 48s^6) \\ & + v^8(2 + 115s^2 + 19s^4 + 152s^6)] \\ & + \frac{\Delta r^5}{48r_0^3\rho^3\chi_0^3\chi^3}[45 - 6v^{12}s^4(4 - 15s^2) \\ & - 3v^2(33 + 61s^2) - v^{10}s^2(13 - 47s^2 + 400s^4) \end{aligned}$$

$$\begin{aligned}
& + 3v^4(23 + 131s^2 + 94s^4) \\
& - 2v^6(5 + 134s^2 + 281s^4 + 108s^6) \\
& + v^8(1 + 53s^2 + 275s^4 + 520s^6). \tag{24d}
\end{aligned}$$

Here  $v^2 := r_0^2 \Omega^2$ ,  $s := \sin \beta$ ,  $\chi := 1 - v^2 s^2$ ,  $\chi_0 := 1 - v^2 = 1/(u^t)^2$ , and

$$\rho := \left[ \frac{2r_0^2 \chi}{\chi_0} (\delta^2 + 1 - \cos \alpha) \right]^{1/2}, \tag{25}$$

with  $\delta^2 := \frac{\chi_0 \Delta r^2}{2r_0^2 \chi}$ . Note that the only dependence of the singular field on  $\alpha$  appears through  $\rho$ , while  $\beta$  appears through  $\rho$ ,  $\chi$ , and the explicit powers of  $s$ . Also note that the above expression for  $\varphi^{\mathcal{P}}(\alpha^{A'})$  is valid only at the instant when the particle is at the north pole of the rotated coordinate system.

Given this choice of puncture field, the residual field is defined implicitly by  $\varphi^{\mathcal{R}} := \varphi^{\text{ret}} - \varphi^{\mathcal{P}}$ . Since we do not have a closed-form expression for  $\varphi^{\text{ret}}$ , we cannot write an exact result for  $\varphi^{\mathcal{R}}$  in 4D. However, we can compute its modes from those of  $\varphi^{\text{ret}}$  and  $\varphi^{\mathcal{P}}$  using  $\varphi_{lm}^{\mathcal{R}} = \varphi_{lm}^{\text{ret}} - \varphi_{lm}^{\mathcal{P}}$ .

Before proceeding, note that in Eq. (23), we have kept the first four orders from the local expansion of  $\varphi^{\mathcal{S}}$ . We refer to this as a fourth-order puncture; if in a particular calculation we include only the first three of them,

we refer to it as a third-order puncture, and so on. The higher the order of the puncture, the smoother the residual field, and hence the more rapid the falloff of  $\varphi_{lm}^{\mathcal{R}}$  with  $l$ . In the following sections we will explore how our strategy of computing  $S$  is impacted by this, and we shall find that the puncture must be of at least third order for our strategy to succeed.

### III. SECOND-ORDER SOURCE

We are now interested in how the modes of the fields are coupled in the source  $S = t^{\mu\nu} \partial_\mu \varphi_1 \partial_\nu \varphi_1$ . For later use, we derive the mode-coupling formula in both  $\theta^A$  and  $\alpha^{A'}$  coordinates. The method of derivation, and the end result in  $\theta^A$  coordinates, was previously presented in Ref. [29], and so we omit some details here.

#### A. In $\theta^A$ coordinates

Written as a bilinear functional,  $S$  is given more explicitly by

$$S[\varphi^{(1)}, \varphi^{(2)}] = \partial_t \varphi^{(1)} \partial_t \varphi^{(2)} + \partial_r \varphi^{(1)} \partial_r \varphi^{(2)} + \frac{1}{r^2} \Omega^{AB} \partial_A \varphi^{(1)} \partial_B \varphi^{(2)}, \tag{26}$$

where  $\varphi^{(1)}$  and  $\varphi^{(2)}$  are any two differentiable fields,  $\Omega_{AB} = \text{diag}(1, \sin^2 \theta)$  is the metric of the unit sphere and  $\Omega^{AB}$  is its inverse. Substituting  $\varphi^{(n)} = \sum_{lm} \varphi_{lm}^{(n)}(r) e^{-im\Omega t} Y_{lm}$ , we get

$$S = \sum_{\substack{l_1 m_1 \\ l_2 m_2}} e^{-i(m_1 + m_2)\Omega t} \left[ (\partial_r \varphi_{l_1 m_1}^{(1)} \partial_r \varphi_{l_2 m_2}^{(2)} - m_1 m_2 \Omega^2 \varphi_{l_1 m_1}^{(1)} \varphi_{l_2 m_2}^{(2)}) Y_{l_1 m_1} Y_{l_2 m_2} + \frac{1}{r^2} \varphi_{l_1 m_1}^{(1)} \varphi_{l_2 m_2}^{(2)} \partial^A Y_{l_1 m_1} \partial_A Y_{l_2 m_2} \right], \tag{27}$$

where indices are raised with  $\Omega^{AB}$ .

To obtain the spherical-harmonic coefficient of Eq. (27), we first rewrite  $\partial_A Y_{lm}$  in terms of spin-weighted harmonics  ${}_s Y_{lm}$  as

$$\partial_A Y^{\ell m} = \frac{1}{2} \sqrt{\ell(\ell+1)} ({}_{-1} Y^{\ell m} m_A - {}_1 Y^{\ell m} m_A^*), \tag{28}$$

where  $m^A := (1, \frac{i}{\sin \theta})$  and its complex conjugate  $m^{*A}$  form a null basis on the unit sphere. This allows us to compute  $S_{lm}$ , which is an integral against  $Y_{lm}^* = {}_0 Y_{lm}^*$ , by appealing to the general formula

$$\oint {}_s Y^{lm*} {}_{s_1} Y^{l_1 m_1} {}_{s_2} Y^{l_2 m_2} d\Omega = C_{l_1 m_1 s_1 l_2 m_2 s_2}^{l m s}, \tag{29}$$

where  $d\Omega = \sin \theta d\theta d\phi$  and for  $s = s_1 + s_2$ ,

$$C_{l_1 m_1 s_1 l_2 m_2 s_2}^{l m s} = (-1)^{m+s} \sqrt{\frac{(2l+1)(2l_1+1)(2l_2+1)}{4\pi}} \begin{pmatrix} l & l_1 & l_2 \\ s & -s_1 & -s_2 \end{pmatrix} \begin{pmatrix} l & l_1 & l_2 \\ -m & m_1 & m_2 \end{pmatrix}. \tag{30}$$

Here the arrays are  $3j$  symbols. If  $s = s_1 = s_2 = 0$ , Eq. (29) reduces to the standard formula for the integral of three ordinary spherical harmonics. We refer the reader to Ref. [29] for more details.

After using Eq. (28),  $m^A m_A = 0$ ,  $m^A m_A^* = 2$ , and Eq. (29), we find that Eq. (27) can be written as  $S = \sum_{lm} S_{lm}(r) e^{-im\Omega t} Y_{lm}$ , with modes given by

$$S_{lm}[\varphi^{(1)}, \varphi^{(2)}] = \sum_{\substack{l_1 m_1 \\ l_2 m_2}} \left[ C_{l_1 m_1 0 l_2 m_2}^{lm0} \left( \partial_r \varphi_{l_1 m_1}^{(1)} \partial_r \varphi_{l_2 m_2}^{(2)} - m_1 m_2 \Omega^2 \varphi_{l_1 m_1}^{(1)} \varphi_{l_2 m_2}^{(2)} \right) - \frac{1}{2r^2} \sqrt{l_1(l_1+1)l_2(l_2+1)} C_{l_1 m_1 -1 l_2 m_2}^{lm0} \left( \varphi_{l_1 m_1}^{(1)} \varphi_{l_2 m_2}^{(2)} + \varphi_{l_1 m_1}^{(2)} \varphi_{l_2 m_2}^{(1)} \right) \right]. \quad (31)$$

We have used the freedom to relabel  $l_1 m_1 \leftrightarrow l_2 m_2$  and the symmetry  $C_{l_1 m_1 s_1 l_2 m_2 s_2}^{lms} = C_{l_2 m_2 s_2 l_1 m_1 s_1}^{lms}$  to slightly simplify this result. We note that the range of the sum is restricted by the  $3j$  symbols in  $C_{l_1 m_1 s_1 l_2 m_2 s_2}^{lms}$ , which enforce (i)  $m = m_1 + m_2$  and (ii) the triangle inequality  $|l_1 - l_2| \leq l \leq l_1 + l_2$ . The first of these restrictions has been used to replace  $e^{-i(m_1+m_2)\Omega t}$  with  $e^{-im\Omega t}$ , and it can be further used to eliminate the sum over  $m_2$ .

In our toy model, Eq. (31) plays the role of Eq. (6) from the gravitational case. When we only have access to a finite number of modes  $\varphi_{lm}^{(n)}$  up to  $l = l_{\max}$ , then the sum is truncated: explicitly, it becomes the partial sum

$$S_{lm}^{l_{\max}} := \sum_{l_1=0}^{l_{\max}} \sum_{l_2=0}^{l_{\max}} \sum_{m_1=-l_1}^{l_1} S_{lm}^{l_1 m_1 l_2, m-m_1}, \quad (32)$$

where we have eliminated the sum over  $m_2$ , and for brevity we have suppressed the functional arguments and defined  $S_{lm}^{l_1 m_1 l_2 m_2}$  as the summand in Eq. (31). By appealing to the triangle inequality, we could write the second sum even more explicitly as  $\sum_{l_2=|l-l_1|}^{\min(l_{\max}, l+l_1)}$ .

The slow convergence of the limit  $S_{lm}^{l_{\max}} \rightarrow S_{lm}$  was illustrated in Fig. 1. Its behavior will be more carefully analyzed in the following sections.

## B. In $\alpha^{A'}$ coordinates

Although Eq. (31) is the mode-coupling formula that we will utilize in explicit computations, we will also make use of the analogous formula in the rotated coordinates  $\alpha^{A'}$ . Deriving that result additionally provides an opportunity to introduce the 4D form of  $S$  in these coordinates, which will be essential in Sec. V.

Obtaining the source in the rotated coordinates involves a new subtlety: the 4D expression for  $S$  involves  $t$  derivatives, while our expression (23) for  $\varphi^{\mathcal{P}}(\alpha^{A'})$  is intended to only be instantaneously valid at the instant when the particle is at the north pole of the rotated coordinate system. We discuss this subtlety in Appendix A. In brief, we may treat the coordinates  $\alpha^{A'}$  as themselves dependent on  $t$ , and appropriately account for that time

dependence when acting with  $t$  derivatives. The 4D expression for  $S$  is then given by Eq. (A4), which we reproduce here for convenience:

$$S[\varphi^{(1)}, \varphi^{(2)}] = \dot{\alpha}^{A'} \partial_{A'} \varphi^{(1)} \dot{\alpha}^{A'} \partial_{A'} \varphi^{(2)} + \partial_r \varphi^{(1)} \partial_r \varphi^{(2)} + \frac{1}{r^2} \Omega^{A'B'} \partial_{A'} \varphi^{(1)} \partial_{B'} \varphi^{(1)}, \quad (33)$$

where  $\Omega^{A'B'} = \text{diag}(1, \csc^2 \alpha)$  is the inverse metric on the unit sphere in the rotated coordinates, and the time derivatives in Eq. (26) now manifest in the quantity  $\dot{\alpha}^{A'} = \Omega(-\cos \beta, \cot \alpha \sin \beta)$ .

The modes of the source in the rotated coordinates are given by

$$S_{lm'} = \oint S(\alpha^{A'}) Y_{lm'}^*(\alpha^{A'}) d\Omega'. \quad (34)$$

We will consistently use  $m'$  to denote the azimuthal number in the rotated coordinates; because  $l$  is invariant under rotations, it is the same in both sets of coordinates.

In Sec. V we will evaluate the integral (34) for  $S[\varphi^{\mathcal{P}}, \varphi^{\mathcal{P}}]$  *without first decomposing  $\varphi^{\mathcal{P}}$  into modes*. But generically, if we expand each  $\varphi^{(n)}$  as  $\sum_{lm'} \varphi_{lm'}^{(n)} Y_{lm'}$ , then we can evaluate the integral analytically in the same way as we did for  $S_{lm}$ . This is made possible by first writing  $\dot{\alpha}^{A'}$  in terms of spin-weight  $\pm 1$  harmonics as

$$\dot{\alpha}^{A'} = \sqrt{\frac{\pi}{3}} \Omega [(-1 Y_{11} +_{-1} Y_{1,-1}) m^{A'} + (1 Y_{11} +_1 Y_{1,-1}) m^{*A'}]. \quad (35)$$

Next, we use Eq. (28), which is covariant on the unit sphere and hence also applies in  $\alpha^{A'}$  coordinates. Combining these results, invoking Eqs. (29)-(30), and using the properties of the  $3j$  symbols to simplify, we find

$$\dot{\alpha}^{A'} \partial_{A'} \varphi = \frac{\Omega}{2} \sum_{lm'} (\mu_{lm'}^- \varphi_{l, m'+1} - \mu_{lm'}^+ \varphi_{l, m'-1}) Y_{lm'}, \quad (36)$$

where  $\mu_{lm'}^\pm := \sqrt{(l \pm m')(l \mp m' + 1)}$ .

Substituting Eq. (36) into Eq. (33) and following the same procedure as in the previous section, we find

$$\begin{aligned}
S_{lm'} = \sum_{\substack{l_1 m'_1 \\ l_2 m'_2}} \left\{ C_{l_1 m'_1 0 l_2 m'_2 0}^{lm'0} \left[ \partial_r \varphi_{l_1 m'_1}^{(1)} \partial_r \varphi_{l_2 m'_2}^{(2)} + \frac{1}{4} \Omega^2 (\mu_1^- \varphi_{l_1, m'_1+1}^{(1)} - \mu_1^+ \varphi_{l_1, m'_1-1}^{(1)}) (\mu_2^- \varphi_{l_2, m'_2+1} - \mu_2^+ \varphi_{l_2, m'_2-1}) \right] \right. \\
\left. - \frac{1}{2r^2} \sqrt{l_1(l_1+1)l_2(l_2+1)} C_{l_1 m'_1 -1 l_2 m'_2 1}^{lm'0} \left( \varphi_{l_1 m'_1}^{(1)} \varphi_{l_2 m'_2}^{(2)} + \varphi_{l_1 m'_1}^{(2)} \varphi_{l_2 m'_2}^{(1)} \right) \right\}, \quad (37)
\end{aligned}$$

where  $\mu_i^\pm := \mu_{l_i m'_i}^\pm$ . Note that unlike Eq. (31), which gave the coefficient in  $\sum_{lm} S_{lm}(r) e^{-im\Omega t} Y_{lm}(\theta^A)$ , Eq. (37) gives the coefficient in  $\sum_{lm} S_{lm'}(r) Y_{lm}(\alpha^{A'})$ , with no phase factor; the time dependence is entirely contained in the  $\alpha^{A'}$  dependence.

#### IV. COMPUTING $S_{lm}[\varphi^{\mathcal{R}}, \varphi^{\mathcal{R}}]$ AND $S_{lm}[\varphi^{\mathcal{R}}, \varphi^{\mathcal{P}}]$

Following the strategy outlined in the introduction, we now compute  $S_{lm}[\varphi^{\mathcal{R}}, \varphi^{\mathcal{R}}]$  and  $S_{lm}[\varphi^{\mathcal{R}}, \varphi^{\mathcal{P}}]$  from the modes of  $\varphi^{\mathcal{R}}$  and  $\varphi^{\mathcal{P}}$  using the mode-coupling formula (31). In Sec. V we will then complete our strategy by computing  $S_{lm}[\varphi^{\mathcal{P}}, \varphi^{\mathcal{P}}]$  from the 4D expression for  $\varphi^{\mathcal{P}}$ .

##### A. Outline of strategy

As input for  $S_{lm}[\varphi^{\mathcal{R}}, \varphi^{\mathcal{R}}]$  and  $S_{lm}[\varphi^{\mathcal{R}}, \varphi^{\mathcal{P}}]$  in Eq. (31), we require the modes  $\varphi_{lm'}^{\mathcal{P}}$ . We begin by computing the modes

$$\varphi_{lm'}^{\mathcal{P}} = \oint \varphi^{\mathcal{P}}(\alpha^{A'}) Y_{lm'}^*(\alpha^{A'}) d\Omega' \quad (38)$$

in the rotated coordinates  $\alpha^{A'}$ . The modes in the unrotated coordinates  $\theta^A$  are then retrieved using

$$\varphi_{lm}^{\mathcal{P}} = \sum_{m'} \varphi_{lm'}^{\mathcal{P}} D_{mm'}^l(\pi, \pi/2, \pi/2), \quad (39)$$

where  $D_{mm'}^l$  is a Wigner  $D$  matrix element. Equation (39) yields the modes in a coordinate system in which the particle is on the equator at an azimuthal angle  $\phi_p = 0$ . An additional rotation brings it to its original position  $\phi_p = \Omega t$ . The sole effect of that rotation is to introduce the phase  $e^{-im\Omega t}$ :  $\varphi_{lm} \rightarrow \varphi_{lm} e^{-im\Omega t}$ .

Given the modes  $\varphi_{lm'}^{\mathcal{P}}$ , the rest of the procedure is straightforward. In summary, it involves four steps:<sup>1</sup>

1. Decompose the puncture field (23) into  $lm'$  modes using Eq. (38).

2. Use Eq. (39) to obtain the  $lm$  modes  $\varphi_{lm}^{\mathcal{P}}$ .
3. Compute the residual-field modes  $\varphi_{lm}^{\mathcal{R}} = \varphi_{lm}^{\text{ret}} - \varphi_{lm}^{\mathcal{P}}$  [with  $\varphi_{lm}^{\text{ret}}$  given in Eqs. (17) and (18)].
4. Use Eq. (31) to compute  $S_{lm}[\varphi^{\mathcal{R}}, \varphi^{\mathcal{R}}]$  and  $S_{lm}[\varphi^{\mathcal{R}}, \varphi^{\mathcal{P}}]$ .

Section IV B describes the first three steps, and Sec. IV C presents and discusses the results of the final step.

##### B. Calculation of $\phi_{lm}^{\mathcal{P}}$

Concretely evaluating the integrals (38) is a nontrivial task. But before addressing that topic, we make several prefatory remarks.

First, we note that although integrals like (38) of local expansions like (23) are common in the literature, in our context they introduce a unique challenge. Typically, integrals of this sort appear in mode-sum regularization and puncture schemes [4, 12]. In those contexts, one's primary goal is to compute the Detweiler-Whiting regular field (or some finite number of its derivatives) on the particle's worldline. This gives one considerable leeway: If one is interested in computing  $n$  derivatives of the regular field, for example, then so long as one preserves the puncture through order  $\lambda^n$ , one can smoothly deform the integrand in Eq. (38), and one can do so in a different way for each  $lm'$  mode. Similarly, one can evaluate the integral with a local expansion in the limit  $\Delta r \rightarrow 0$ , which generally simplifies the integration. And since  $Y_{lm'}$  vanishes at  $\alpha = 0$  for  $m' \neq 0$ , one need only evaluate the  $m' = 0$  mode (or in the calculations in Ref. [32], the  $m' = 0, \pm 1, \pm 2$  modes); traditionally, this restriction to  $m' = 0$  has been a major advantage of using rotated coordinates like  $\alpha^{A'}$ .

In our calculation, we have none of these luxuries. Because we compute  $S_{lm}[\varphi^{\mathcal{P}}, \varphi^{\mathcal{P}}]$  from the 4D expression for  $\varphi^{\mathcal{P}}$  while we compute  $S_{lm}[\varphi^{\mathcal{R}}, \varphi^{\mathcal{P}}]$  and  $S_{lm}[\varphi^{\mathcal{R}}, \varphi^{\mathcal{R}}]$  from the modes  $\varphi_{lm'}^{\mathcal{P}}$ , the modes must correspond to an *exact* evaluation of Eq. (38); otherwise,  $S_{lm}[\varphi^{\mathcal{P}}, \varphi^{\mathcal{P}}] + 2S_{lm}[\varphi^{\mathcal{R}}, \varphi^{\mathcal{P}}] + S_{lm}[\varphi^{\mathcal{R}}, \varphi^{\mathcal{R}}]$  would not be equal to  $S_{lm}[\varphi^{\text{ret}}, \varphi^{\text{ret}}]$ . This means that if we deform the integrand in Eq. (38), then we must make an identical deformation of the 4D expression for  $\varphi^{\mathcal{P}}$ . Similarly, any expansion in powers of  $\Delta r$  would have to be performed for both the  $lm'$  modes and the 4D expression; because we must evaluate these quantities over a range of  $\Delta r$  values,

<sup>1</sup> We could alternatively compute the modes  $S_{lm'}[\varphi^{\mathcal{R}}, \varphi^{\mathcal{R}}]$  and  $S_{lm'}[\varphi^{\mathcal{R}}, \varphi^{\mathcal{P}}]$  directly from  $\varphi_{lm'}^{\mathcal{P}}$  using Eq. (37).  $S_{lm}[\varphi^{\mathcal{R}}, \varphi^{\mathcal{R}}]$  and  $S_{lm}[\varphi^{\mathcal{R}}, \varphi^{\mathcal{P}}]$  would then be computed using the analogs of Eq. (39).



we cannot rely on eventually taking the limit  $\Delta r \rightarrow 0$ . And finally, we cannot limit our computation to  $m' = 0$ ; since we do not evaluate any quantities at  $\alpha = 0$ , there is no *a priori* limit to the number of  $m'$  modes we must compute. (If we only required  $S$  on the particle, then we would only require the modes  $S_{l0'}$ , but even these modes depend on all  $m'$  modes of  $\varphi$ .)

In brief, we must be exact. We must compute all  $lm'$  modes of  $\varphi^{\mathcal{P}}$  without introducing any approximations. The lone exception to this, to be discussed in Sec. IV C 1, is that in practice we can truncate the number of  $m'$  modes at some  $|m'| = m'_{\max}$ . This is possible because the modes fall rapidly with  $|m'|$ , allowing us to neglect large- $|m'|$  modes without introducing significant numerical error.

We must address one more issue before detailing the evaluation of Eq. (38). As discussed in Ref. [32], our puncture  $\varphi^{\mathcal{P}}$  is *not* smooth at all points off the particle. The particle sits at the north pole  $\alpha = 0$  of the sphere at  $\Delta r = 0$ , and  $\varphi^{\mathcal{P}}$  correctly diverges as  $1/\lambda$  there. But even away from the particle, for each fixed  $\Delta r \neq 0$ ,  $\varphi^{\mathcal{P}}$  has a directional discontinuity at the south pole  $\alpha = \pi$ , inherited from a directional discontinuity in the quantity  $\rho$ . This discontinuity is nonphysical.  $\varphi^{\mathcal{P}}$  is originally defined from a local expansion in the neighbourhood of the particle, but in order to evaluate the integrals (38), it must be extended over the entire sphere spanned by  $\alpha^A$ . The particular discontinuity we face is a consequence of the particular manner in which we have performed that extension. Because the total field  $\varphi^{\mathcal{P}} + \varphi^{\mathcal{R}}$  is smooth at all points off the particle, this singularity at  $\alpha = \pi$  must be cancelled by one in  $\varphi^{\mathcal{R}}$ . And because nonsmoothness of a field leads to slow falloff with  $l$ , this discontinuity limits the convergence rate of  $S_{lm}[\varphi^{\mathcal{R}}, \varphi^{\mathcal{R}}]$  and  $S_{lm}[\varphi^{\mathcal{R}}, \varphi^{\mathcal{R}}]$  with  $l_{\max}$ . Concretely, the discontinuity introduces terms of the form  $\frac{(-1)^l}{l}$  into  $\varphi_{lm'}^{\mathcal{R}}$  for all  $m' \neq 0$ .

To eliminate the discontinuity, we must adopt a different extension of  $\varphi^{\mathcal{P}}$  over the sphere. Following Ref. [32], we do so by introducing a regularizing factor:

$$\varphi^{\mathcal{P}}(\Delta r, \alpha^{A'}) \rightarrow \mathcal{W}_m^n(\cos \alpha) \varphi^{\mathcal{P}}(\Delta r, \alpha^{A'}). \quad (40)$$

Here the parameters  $n$  and  $m$  are chosen such that  $n \geq k$  and  $m \geq m'_{\max}$ , where  $k$  is the order of the puncture and  $m'_{\max}$  is the maximum value of  $|m'|$  we use.  $\mathcal{W}_m^n$ 's dependence on these two parameters is dictated by the required behavior at the two poles. To control the behavior at the south pole, we choose a regularizing factor that scales as  $\mathcal{W}_m^n = \mathcal{O}[(\pi - \alpha)^m]$ , which makes  $\mathcal{W}_m^n \varphi^{\mathcal{P}}$  a  $C^{m-1}$  function at  $\alpha = \pi$ . For an otherwise smooth function, standard estimation methods [39] show that this degree of smoothness ensures that the modes  $|\varphi_{lm'}^{\mathcal{P}}|$ , and hence  $|\varphi_{lm'}^{\mathcal{R}}|$ , fall off as  $\lesssim l^{-m \pm 1}$ ; for sufficiently large  $m$ , this nonspectral decay will be negligible compared to the slow convergence coming from the singularity at the particle. Now, at the same time as satisfying these conditions at the south pole, we must keep control of the behavior at the north pole. Specifically,  $\mathcal{W}_m^n$  must leave all  $k$  orders intact in the  $k$ th-order puncture, implying that it must

behave as  $\mathcal{W}_m^n = 1 + \mathcal{O}(\alpha^n)$  near  $\alpha = 0$ . We satisfy the requirements at both poles by choosing

$$\begin{aligned} \mathcal{W}_m^n := & 1 - \frac{n}{2} \binom{(m+n-2)/2}{n/2} \\ & \times B\left(\frac{1-\cos \alpha}{2}; \frac{n}{2}, \frac{m}{2}\right), \end{aligned} \quad (41)$$

where  $\binom{p}{q}$  is the Binomial coefficient, and  $B(z; a, b)$  is the incomplete Beta function.

This choice has the required properties at the poles provided  $n$  and  $m$  are positive integers, and additionally that  $m$  is even. This is not a significant restriction; as discussed below, the  $\beta$  integrals ensure that only even  $m'$  need be considered in our circular-orbit toy model, and even if this were not the case we could always choose  $m$  to be the smallest even number greater than  $m'_{\max}$ . With these restrictions on  $n$  and  $m$ ,  $\mathcal{W}_m^n$  takes the straightforward form of a polynomial in  $y := \frac{1-\cos \alpha}{2}$ , whose coefficients and degree both depend on the particular choice of  $n$  and  $m$ . For example, in all our computations we use  $n = 4$  (equal to the highest order of puncture we use) and  $m = 10$  (equal to the value of  $m'_{\max}$  we almost exclusively use), in which case  $\mathcal{W}_{10}^4 = 1 - 15y^2 + 40y^3 - 45y^4 + 24y^5 - 5y^6$ .

Heeding the warnings above about our need for exactness, we must apply this regularization consistently to the 4D puncture in all our calculations, not solely in evaluating the integrals (38). So henceforth, we will always use Eq. (40) as our puncture, with fixed  $n$  and  $m$  independent of the particular  $l, m'$  mode being considered.

With our preparations out of the way, we now describe our evaluation of the integrals (38). We use two methods for computing the double integral (38), namely (i) evaluate the  $\alpha$  integrals analytically and subsequently evaluate the  $\beta$  integrals as numerical elliptic-type integrals, and (ii) evaluate both the  $\alpha$  and  $\beta$  integrals entirely numerically. The second method is computationally more expensive than the first. However, we used both methods as an internal consistency check. We will describe method (i) first and begin by explaining the steps in the analytical evaluation of the  $\alpha$  integrals.

### 1. Integration over alpha

We first recall that all of the  $\alpha$  dependence of the puncture (24) is contained inside the quantity  $\rho$ . Hence, the integral that we need to evaluate takes the general form

$$\int_{-1}^1 \mathcal{W}_m^k(x) P_l^{m'}(x) \rho^n dx, \quad (42)$$

where  $x = \cos \alpha$ ,  $P_l^{m'}(x)$  are the associated Legendre polynomials, and  $n$  is an odd integer.

Furthermore, the simple form of  $\mathcal{W}_m^n$  as a power series in  $\frac{1-\cos \alpha}{2}$  means that we can use Eq. (25) to rewrite it

as an even power series in  $\Delta r$  and  $\rho$ . The integrals (42)

can therefore all be written in the form

$$\int_{-1}^1 P_l^{m'}(x) \rho^n dx \quad (43)$$

for  $n$  an odd integer.

Concentrating first on the simplest case of  $m' = 0$ , the integration can be done analytically using

$$\begin{aligned} & \int_{-1}^1 (\delta^2 + 1 - x)^{n/2} P_\ell^0(x) dx \\ &= \frac{(-1)^{\frac{n+1}{2}} (\delta^2 + 2)^{\frac{n}{2}+1} \left[ \left( \frac{1}{2} \right)_{\frac{n+1}{2}} \right]^2}{\left( l - \frac{n}{2} \right)_{n+2}} {}_2F_1\left(-l, l+1; -\frac{n}{2}; -\frac{\delta^2}{2}\right) - \frac{2|\delta| \delta^{n+1}}{n+2} {}_2F_1\left(-l, l+1; \frac{n}{2}+2; -\frac{\delta^2}{2}\right) \\ &= \frac{(-1)^{\frac{n+1}{2}} (\delta^2 + 2)^{\frac{n}{2}+1} \left[ \left( \frac{1}{2} \right)_{\frac{n+1}{2}} \right]^2}{\left( l - \frac{n}{2} \right)_{n+2}} \sum_{k=0}^l \frac{(-1)^k \delta^{2k} (l-k+1)_{2k}}{2^k k! \left( \frac{n}{2} - k + 1 \right)_k} - |\delta| \delta^{n+1} \sum_{k=0}^l \frac{\delta^{2k} (l-k+1)_{2k}}{2^k k! \left( \frac{n}{2} + 1 \right)_{k+1}}. \end{aligned} \quad (44)$$

For any given odd integer  $n$ , this is merely a pair of even polynomials of degree  $2l$  in  $\delta$ , one multiplying  $(\delta^2 + 2)^{\frac{n}{2}+1}$  and the other multiplying  $|\delta| \delta^{n+1}$ .

Turning to the  $m' \neq 0$  case, these can now be written in terms of the  $m' = 0$  result. Using the definition for the associated Legendre polynomials in terms of the Legendre polynomials,

$$P_l^{m'}(x) = (-1)^m (1-x^2)^{m/2} \frac{d^m}{dx^m} P_l(x), \quad (45)$$

the integral (43) can be integrated by parts  $m'$  times, resulting in an integral of the form (44) along with a set of  $m'$  boundary terms. These boundary terms are given by

$$\sum_{k=0}^{m'-1} \left[ (-1)^k \frac{d^k \rho^n}{dx^k} \frac{d^{m'-k-1}}{dx^{m'-k-1}} P_l(x) \right]_{x=-1}^{x=1}, \quad (46)$$

and are therefore power series in  $\delta$  of the same kind as in Eq. (44). The integrals over  $\beta$  then have the same form as for the  $m' = 0$  case.

## 2. Alternative method for evaluating $\alpha$ integrals

An alternative, but equivalent strategy for evaluating the  $\alpha$  integrals, Eq. (42), is based on expressing  $\mathcal{W}_m^n(x)$  and  $P_l^{m'}(x)$  as finite polynomials in  $(1+x)$  and  $(1-x)$ . For example  $n = 4$  and  $m = 10$ , Eq. (41) can be written as

$$\mathcal{W}_{10}^4(x) = \frac{3}{16}(1+x)^5 - \frac{5}{64}(1+x)^6. \quad (47)$$

Similarly, for  $m \geq 0$ ,

$$\begin{aligned} P_l^m(x) &= \sum_{p=0}^l \sum_{q=0}^m c_{lmpq} (1+x)^{p+q-m/2} \\ &\quad \times (1-x)^{l-p-q+m/2}, \end{aligned} \quad (48)$$

where  $c_{lmpq}$  are  $x$ -independent constants given by

$$\begin{aligned} c_{lmpq} &= \frac{(-1)^{m+l-p+q}}{2^l} \binom{l}{p}^2 \binom{m}{q} \\ &\quad \times \frac{(l-p)!}{(l-p-q)!} \frac{p!}{(p-m+q)!}. \end{aligned} \quad (49)$$

Equation (48) can be derived by using the standard representation  $P_l(x) = \frac{1}{2^l} \sum_{p=0}^l \binom{l}{p}^2 (x-1)^{l-p} (x+1)^p$  in the formula  $P_l^m = (-1)^m (1-x^2)^{m/2} \frac{d^m}{dx^m} P_l(x)$  and appealing to the Leibniz rule. The analogue of Eq. (48) for  $m < 0$  follows from  $P_l^{-m} = (-1)^m \frac{(l-m)!}{(l+m)!} P_l^m$ ; but in practice we need not evaluate the integrals (42) for  $m' < 0$ , since for real-valued  $\varphi^P$  we have  $\varphi_{l,-m'}^P = (-1)^{m'} \varphi_{lm'}^{P*}$ .

Substituting the polynomials (47) and (48) into (42) yields a sum of integrals of the form  $F_{abn}(\delta) := \int_{-1}^1 dx (1+x)^{a/2} (1-x)^{b/2} (\delta^2 + 1 - x)^{n/2}$ , where  $a, b, n$  are positive integers. We write the  $\alpha$  integral in Eq. (38) as a linear combination of these integrals  $F_{abn}$ . Using Wolfram Mathematica, we tabulate analytical formulae for all  $F_{abn}$  that appear in this linear combination for  $\varphi_{lm'}^P$  to  $l = 200$  and  $m' = 10$ . Each of the tabulated formulae is a finite polynomial in  $\delta$ , and once tabulated, these formulae allow us to almost instantaneously evaluate the  $\alpha$  integral.

### 3. Integration over $\beta$

We next turn to computing the  $\beta$  integrals. The explicit  $\beta$ -dependent terms in the puncture, Eq. (24), appear in the form of positive, even powers of  $\sin \beta$ . The other dependences on  $\beta$  in the integrand appear through  $\rho$  (where they appear as powers of  $\chi = 1 - r_0^2 \Omega^2 \sin^2 \beta$ ), through  $\chi$  itself, and through the factor of  $e^{-im'\beta}$  from the spherical harmonic. With this in mind it can readily be shown that odd- $m'$  modes vanish and all of the non-vanishing modes are purely real.

Furthermore, following from this structure the net dependence on  $\beta$  has two possible forms. The first term in Eq. (44) above yields integrals of the form

$$\int_0^{2\pi} \left(2 + \frac{\chi_0 \Delta r^2}{2r_0^2 \chi}\right)^{\frac{n}{2}+1} \chi^{k/2} d\beta, \quad (50)$$

where  $n$  is an odd integer. For  $n = -1$  and  $k = -1$  this can be recognized as a complete elliptic integral of the third kind, with arguments that depend on  $\Delta r$ ,  $r_0$ , and  $\Omega$  (through  $\chi_0$ ). All other values of  $n$  and  $k$  can be reduced to this case by integrating by parts a sufficient number of times. The second type of integral arises from the second term in Eq. (44). This yields integrands involving  $\chi^n$  with  $n$  an integer; their integral is a polynomial involving  $r_0 \Omega$ . Combining these results, we can therefore compute the integrals over  $\beta$  exactly and analytically (in terms of elliptic integrals).

In practice we found it sufficiently efficient (and simpler) to evaluate the  $\beta$  integral directly using numerical integration, rather than manipulating it into elliptic integral form. In that case, we used the fact that the integrand is symmetric in the sense that

$$\int_0^{2\pi} f(\beta)_{lm'} d\beta = 2 \int_0^\pi f(\beta)_{lm'} d\beta \quad (51)$$

to reduce the computational cost. To compute the integrals we used a C++ code employing a 15-point Gauss-Kronrod rule.

### 4. Two-dimension numerical integration

As a check on our methods, we also evaluated Eq. (38) by computing the double integral entirely numerically. We used a C++ code employing a 25-point Clenshaw-Curtis integration rule. As the azimuthal mode number  $m'$  increases, the  $\beta$  integrals become highly oscillatory, resulting in loss of accuracy. We found that to improve the accuracy of our results, it was necessary to split the  $\beta$  integral, over the range  $[0, \pi]$ , into a sum of  $m'$  separate integrals, each over the range  $\beta \in [(i-1)/(m'\pi), i/(m'\pi)]$ , where  $i$  runs from 1 to  $m'$ . In all cases, this fully numerical method agreed with the mixed analytical-numerical method described above.

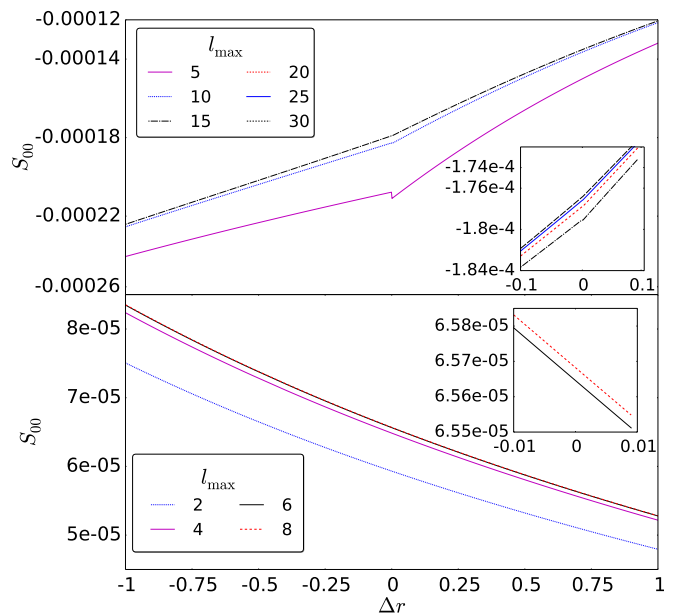


FIG. 3. Demonstration of rapid convergence of the sum (31) for  $S_{00}[\varphi^{\mathcal{R}}, \varphi^{\mathcal{P}}]$  (top panel) and  $S_{00}[\varphi^{\mathcal{R}}, \varphi^{\mathcal{R}}]$  (bottom panel). The mode  $S_{00}$  is plotted as a function of  $\Delta r$  for a range of values of  $l_{\max}$ . Here we use  $r_0 = 10$ ,  $m'_{\max} = 10$ , and all four orders in the puncture (23).

### C. Calculation of $S_{lm}[\varphi^{\mathcal{R}}, \varphi^{\mathcal{R}}]$ and $S_{lm}[\varphi^{\mathcal{R}}, \varphi^{\mathcal{P}}]$

After obtaining the modes of  $\varphi^{\mathcal{P}}$ , we implement the final three steps in the strategy outlined at the end of Sec. IV A. The results are shown in Fig. 3 for the monopole modes  $S_{00}[\varphi^{\mathcal{R}}, \varphi^{\mathcal{P}}]$  and  $S_{00}[\varphi^{\mathcal{R}}, \varphi^{\mathcal{R}}]$ . We see that unlike  $S_{lm}[\varphi^{\text{ret}}, \varphi^{\text{ret}}]$ ,  $S_{lm}[\varphi^{\mathcal{R}}, \varphi^{\mathcal{P}}]$  and  $S_{lm}[\varphi^{\mathcal{R}}, \varphi^{\mathcal{R}}]$  both converge rapidly with increasing  $l_{\max}$ . On the scale of the main plot,  $S_{lm}[\varphi^{\mathcal{R}}, \varphi^{\mathcal{P}}]$  has numerically converged by  $l_{\max} = 10$  and  $S_{lm}[\varphi^{\mathcal{R}}, \varphi^{\mathcal{R}}]$  by  $l_{\max} = 6$ ; the insets show the small changes at larger  $l_{\max}$ .

However, to make useful predictions about how our strategy extends to gravitational fields, we must say more than that it works; we must say something about how and when it works. We do this by considering two important convergence properties of Eq. (31):

1. How quickly do  $S_{lm}[\varphi^{\mathcal{R}}, \varphi^{\mathcal{P}}]$  and  $S_{lm}[\varphi^{\mathcal{R}}, \varphi^{\mathcal{R}}]$  converge as  $m'_{\max} \rightarrow \infty$ ?
2. How does the convergence of  $S_{lm}[\varphi^{\mathcal{R}}, \varphi^{\mathcal{P}}]$  and  $S_{lm}[\varphi^{\mathcal{R}}, \varphi^{\mathcal{R}}]$  with  $l_{\max}$  depend on the order of the puncture  $\varphi^{\mathcal{P}}$ ? More pointedly, how high order must the puncture be in order to guarantee convergence with  $l_{\max}$ ?

The last of these is the most pertinent: as we shall discuss below, if the puncture is of too low order, then our strategy simply does not work. However, to elucidate that issue, it will be useful to first determine the convergence with  $m'_{\max}$ .

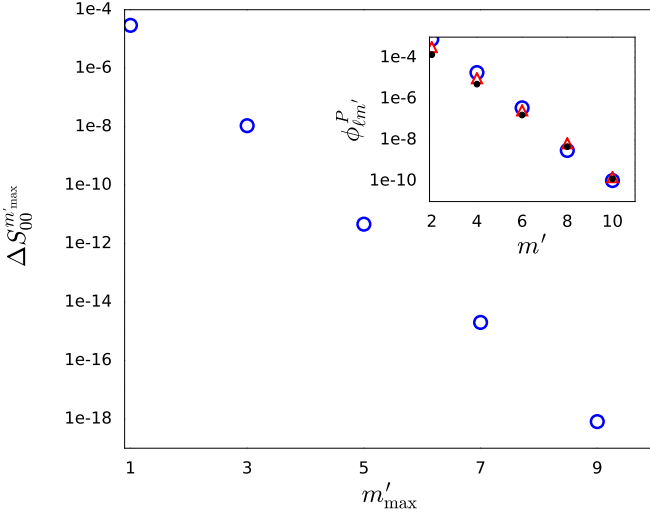


FIG. 4. Influence of  $m'$  modes on  $S_{lm}$ . The main plot shows  $\Delta S_{00}^{m'_{\max}}[\varphi^{\mathcal{R}}, \varphi^{\mathcal{R}}]$ , which is seen to fall off linearly on the plot's semilog scale, implying exponential decay with  $m'_{\max}$ . The inset shows  $\varphi_{lm'}^{\mathcal{P}}$  as a function of  $m'$  for  $l = 10$  (open blue circles),  $l = 20$  (closed black circles), and  $l = 30$  (open red triangles). In all cases, the modes decay exponentially with  $m'$ ; this behavior carries over to  $\varphi_{lm'}^{\mathcal{R}}$  and explains the falloff of  $\Delta S_{00}^{m'_{\max}}$ . To obtain this data we used a fourth-order puncture,  $l_{\max} = 30$ , and  $\Delta r = 10^{-4}$ .

### 1. Convergence with $m'_{\max}$

To assess the rate of convergence with  $m'_{\max}$ , we introduce the finite difference

$$\Delta S_{lm}^{m'_{\max}} := S_{lm}^{m'_{\max}} - S_{lm}^{m'_{\max}-1}, \quad (52)$$

where  $S_{lm}^{m'_{\max}}$  is given by Eq. (31) with  $\varphi_{lm'}^{(1)}$  and  $\varphi_{lm'}^{(2)}$  set to zero for  $|m'| > m'_{\max}$ . Concretely, this means truncating the sum (39) at  $|m'| = m'_{\max}$ .

Figure 4 displays the quantity  $\Delta S_{00}^{m'_{\max}}[\varphi^{\mathcal{R}}, \varphi^{\mathcal{R}}]$  as a function of  $m'_{\max}$  at a fixed value of  $l_{\max}$  and  $\Delta r$ . On the semilogarithmic scale of the plot,  $\Delta S_{00}^{m'_{\max}}$  falls linearly, indicating exponential decay. Although we do not display it, the behavior of  $\Delta S_{00}^{m'_{\max}}[\varphi^{\mathcal{R}}, \varphi^{\mathcal{P}}]$  is identical, and the behavior is independent of  $\Delta r$ . Given this rapid decay, we conclude that in practice, we need include only a small number of  $m'$  modes; in all other figures in this paper, we use  $m'_{\max} = 10$ .

$S_{lm}$ 's rapid convergence with  $m'_{\max}$  is a consequence of  $\varphi_{lm'}^{\mathcal{P}}$ 's rapid falloff with  $m'$ . As shown in the inset of Fig. 4, this falloff is exponential, like that of  $\Delta S_{lm}^{m'_{\max}}$ . The exponential falloff naturally extends from  $\varphi_{lm'}^{\mathcal{P}}$  to  $\varphi_{lm'}^{\mathcal{R}}$ , since  $\varphi^{\text{ret}}$  will never possess worse convergence properties than  $\varphi^{\mathcal{P}}$ , and from there it extends to the convergence of the sum (39) and finally to Eq. (31).

We can best understand this behavior, and predict its extension to the gravity case, by obtaining analyt-

ical estimates of  $\varphi_{lm'}^{\mathcal{P}}$ 's falloff. First consider the decomposition into  $m'$  modes, without the attendant decomposition into  $l$  modes. An  $m'$  mode is defined by  $\varphi_{m'}^{\mathcal{P}} = \int_0^{2\pi} e^{-im'\beta} \varphi^{\mathcal{P}} d\beta$ . For all  $\alpha \neq 0$ , we can integrate by parts  $p$  times to express this as

$$\varphi_{m'}^{\mathcal{P}} = \left(\frac{-i}{m'}\right)^p \int_0^{2\pi} e^{-im'\beta} \partial_{\beta}^p \varphi^{\mathcal{P}} d\beta. \quad (53)$$

Hence,

$$|\varphi_{m'}^{\mathcal{P}}| \leq \frac{C(\Delta r, \alpha)}{|m'|^p}, \quad (54)$$

where  $C(\Delta r, \alpha) := 2\pi \max_{\beta} |\partial_{\beta}^p \varphi^{\mathcal{P}}|$  is independent of  $m'$ . Since  $\varphi^{\mathcal{P}}$  is a  $C^{\infty}$  function of  $\beta$  at each fixed  $\alpha \neq 0, \pi$ , the bound (54) holds for all integers  $p \geq 0$ , and we can see by induction that  $\varphi_{m'}^{\mathcal{P}}$  falls faster than any inverse power of  $|m'|$ . This rate is uniform in  $\Delta r$  for each  $\alpha \neq 0, \pi$ ; it is not uniform in  $(\Delta r, \alpha)$  because the divergence at the particle implies  $\sup C(\Delta r, \alpha) = \infty$ .

Now consider the decomposition into  $lm'$  modes, which we may write as  $\varphi_{lm'}^{\mathcal{P}} = N_{lm'} \int_0^{\pi} \varphi_{m'}^{\mathcal{P}} P_l^{m'}(\cos \alpha) \sin \alpha d\alpha$ , where  $N_{lm'} = \sqrt{\frac{2l+1}{4\pi} \frac{(l-m')!}{(l+m')!}}$ . Because the exponential falloff of  $\varphi_{m'}^{\mathcal{P}}$  is nonuniform, we might worry that it does not extend to  $\varphi_{lm'}^{\mathcal{P}}$ . However, we can quickly deduce that that is not the case. Using the bound [40]  $|N_{lm'} P_l^{m'}| \leq \sqrt{\frac{2l+1}{8\pi}}$  and Eq. (53), we have

$$|\varphi_{lm'}^{\mathcal{P}}| \leq \frac{1}{|m'|^p} \sqrt{\frac{2l+1}{8\pi}} \int_0^{\pi} \int_0^{2\pi} |\partial_{\beta}^p \varphi^{\mathcal{P}} \sin \alpha| d\alpha. \quad (55)$$

Next we note that  $\partial_{\beta}^p \varphi^{\mathcal{P}}$  has the same behavior as  $\varphi^{\mathcal{P}}$ : it is finite except at  $\Delta r = 0$ , where it diverges as  $\sim 1/\alpha$  at small  $\alpha$ ; the derivatives with respect to  $\beta$  do not alter this behavior. Hence, the  $lm'$ -independent integral  $\int_0^{\pi} \int_0^{2\pi} |\partial_{\beta}^p \varphi^{\mathcal{P}} \sin \alpha| d\alpha$  exists for all integers  $p \geq 0$ , and we infer by induction that  $\varphi_{lm'}^{\mathcal{P}}$  falls off faster than any power of  $|m'|$ . Of course, we can only consider large  $m'$  if  $l$  is at least as large. But because the only  $l$  dependence in the bound (55) is the factor  $\sqrt{2l+1}$ , this consideration does not affect our conclusion.

Of course, exponential convergence does not necessarily mean usefully fast convergence. As we have seen, the falloff of  $\varphi_{lm}^{\mathcal{P}}$  with  $l$  is exponentially fast at all points away from  $\Delta r = 0$ , but for practical purposes it is slow for small  $\Delta r$ . However, that is an artefact of the convergence rate being nonuniform. Crucially, the convergence with  $m'_{\max}$  is uniform in  $\Delta r$ .

The (uniformly) rapid falloff of  $\Delta S_{lm}^{m'_{\max}}[\varphi^{\mathcal{R}}, \varphi^{\mathcal{P}}]$  and  $\Delta S_{lm}^{m'_{\max}}[\varphi^{\mathcal{R}}, \varphi^{\mathcal{R}}]$  with  $m'_{\max}$  now follows directly from the rapid falloff of  $\varphi_{lm'}^{\mathcal{P}}$ . Because this conclusion relies only on generic behavior of the puncture, it will also apply in the gravity case.

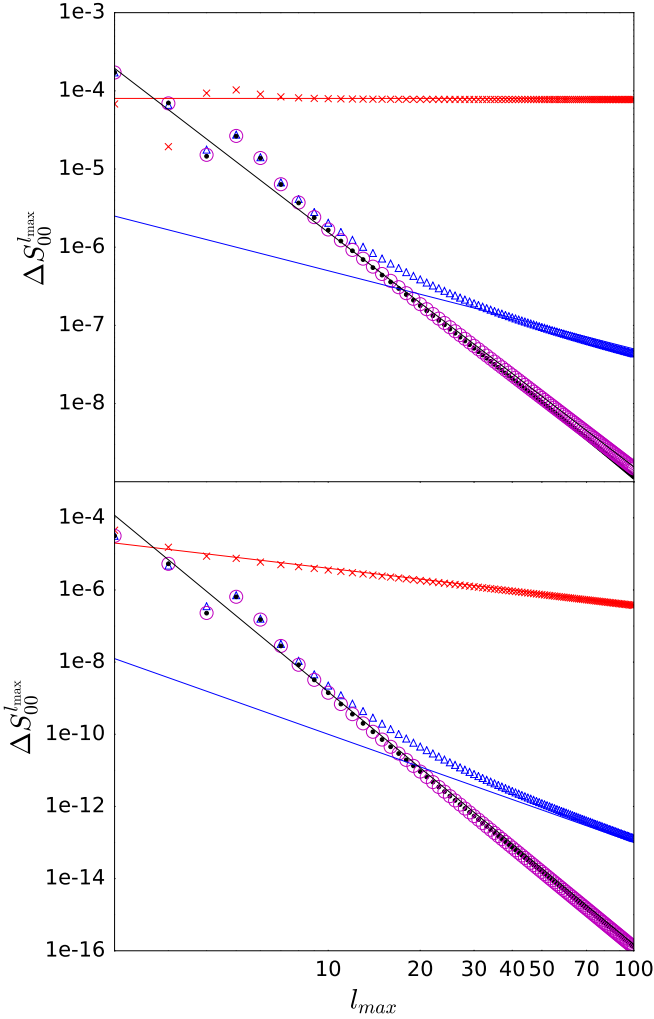


FIG. 5. The impact of the puncture order  $k$  on  $S_{lm}$ 's convergence with  $l_{\max}$ .  $\Delta S_{00}^{l_{\max}}[\varphi^{\mathcal{R}}, \varphi^{\mathcal{P}}]$  (top panel) and  $\Delta S_{00}^{l_{\max}}[\varphi^{\mathcal{R}}, \varphi^{\mathcal{P}}]$  (bottom) are plotted as functions of  $l_{\max}$ . In both panels, results are shown for  $k = 1$  (red crosses),  $k = 2$  (blue triangles),  $k = 3$  (solid black circles), and  $k = 4$  (open purple circles) and  $\Delta r = 10^{-12}$ . The straight lines show the asymptotic behavior  $\propto l_{\max}^p$  of the data. In the top panel, listed from top to bottom, they are proportional to  $l_{\max}^0$ ,  $l_{\max}^{-1}$ , and  $l_{\max}^{-3}$ ; in the bottom panel,  $l_{\max}^{-1}$ ,  $l_{\max}^{-3}$ , and  $l_{\max}^{-7}$ .

## 2. Convergence with $l_{\max}$

We now turn to the central issue of the convergence rate with  $l_{\max}$ . To assess that, we examine the finite difference

$$\Delta S_{lm}^{l_{\max}} := S_{lm}^{l_{\max}} - S_{lm}^{l_{\max}-1}, \quad (56)$$

where  $S_{lm}^{l_{\max}}$  is the partial sum in Eq. (32).

Figure 5 displays  $\Delta S_{00}^{l_{\max}}[\varphi^{\mathcal{R}}, \varphi^{\mathcal{P}}]$  and  $\Delta S_{00}^{l_{\max}}[\varphi^{\mathcal{R}}, \varphi^{\mathcal{P}}]$  at a point very near the particle ( $\Delta r = 10^{-12}$ ). We see that when so close to the particle, the sum (31) exhibits power law convergence. At large enough  $l_{\max}$ , this will morph into exponential convergence, as  $\varphi_{lm}$ 's slow expo-

ponential decay with  $l$  eventually takes over. The further we move from the particle, the less clean the power laws, and the more quickly the exponential convergence dominates.

The most important aspect of the power laws are their dependence on the order of the puncture. As we will discuss below, a subtle competition between power laws makes determining the true asymptotics nontrivial, and the numerical results can be misleading. Nevertheless, the numerics provide a useful frame for the discussion. For a  $k$ th-order puncture, Fig. 5 suggests that  $S_{00}[\varphi^{\mathcal{R}}, \varphi^{\mathcal{P}}]$  converges as

$$\Delta S_{00}^{l_{\max}}[\varphi^{\mathcal{R}}, \varphi^{\mathcal{P}}] \sim \begin{cases} l_{\max}^{-1} & \text{if } k = 1, \\ l_{\max}^{-3} & \text{if } k = 2, \\ l_{\max}^{-7} & \text{if } k = 3 \text{ or } 4; \end{cases} \quad (57)$$

we will demonstrate below that for  $k = 3$ , this inferred falloff is incorrect, and that one would have to go to much larger values of  $l_{\max}$  to see the true asymptotic behavior. But the essential facts are unaltered by that: In order for  $S_{lm}$  to converge with  $l_{\max}$ ,  $\Delta S_{lm}^{l_{\max}}$  must fall off at least as  $l_{\max}^{-1-p}$  with  $p > 0$ . Hence, to ensure numerical convergence of  $S_{00}[\varphi^{\mathcal{R}}, \varphi^{\mathcal{P}}]$ , we must use at least a second-order puncture. Although exponential convergence would eventually manifest, in a concrete situation where we have access to modes up to  $l = l_{\max}$ , the exponential convergence would only assist us at distances  $|\Delta r| \sim r_0$  from the particle.

Because  $\varphi^{\mathcal{P}}$  is singular,  $S_{00}[\varphi^{\mathcal{R}}, \varphi^{\mathcal{P}}]$  converges more slowly than  $S_{00}[\varphi^{\mathcal{R}}, \varphi^{\mathcal{R}}]$ . According to Fig. 5,

$$\Delta S_{00}^{l_{\max}}[\varphi^{\mathcal{R}}, \varphi^{\mathcal{P}}] \sim \begin{cases} l_{\max}^0 & \text{if } k = 1, \\ l_{\max}^{-1} & \text{if } k = 2, \\ l_{\max}^{-3} & \text{if } k = 3 \text{ or } 4; \end{cases} \quad (58)$$

again, the inferred falloff for  $k = 3$  is incorrect. But again, we can nevertheless draw the essential conclusions: Because they are slower than those of Eq. (57), the falloff rates in Eq. (58) are the ultimate determiner of how high order our puncture must be. To ensure numerical convergence of  $S_{00}[\varphi^{\mathcal{R}}, \varphi^{\mathcal{R}}] + 2S_{00}[\varphi^{\mathcal{R}}, \varphi^{\mathcal{P}}]$ , and hence to allow our overarching strategy to succeed, we must use at least a third-order puncture.

All of the behavior we have just described is generic; it is not particular to the monopole. We now argue, by way of scaling estimates for arbitrary  $k$ , that it also extends to the gravitational case. As a byproduct of our derivation, we will also discover, as alluded to above, that the power laws in Eqs. (57) and (58) are not the true asymptotic falloffs for  $k = 3$ .

First let us continue to focus on  $S_{00}$ . We will afterward generalize to arbitrary  $lm$ . Although in practice we use Eq. (31) to compute  $S_{lm}$ , Eq. (37) will be more useful for our argument. For  $l = 0$ , Eq. (30) simplifies to

$$C_{l_1 m_1 s_1 l_2 m_2 s_2}^{000} = \frac{(-1)^{m_1+s_1}}{\sqrt{4\pi}} \delta_{l_2}^{l_1} \delta_{-m_2}^{m_1} \delta_{-s_2}^{s_1}, \quad (59)$$

where  $\delta_j^i$  is a Kronecker delta. Substituting this into Eq. (37) and simplifying, we find

$$S_{00} = \frac{1}{\sqrt{4\pi}} \sum_{lm'} \left[ \partial_r \varphi_{lm'}^{(1)} \partial_r \varphi_{lm'}^{(2)*} + \frac{l(l+1)}{r^2} \varphi_{lm'}^{(1)} \varphi_{lm'}^{(2)*} + \frac{\Omega^2}{4} (\mu_{lm'}^- \varphi_{l,m'+1}^{(1)} - \mu_{lm'}^+ \varphi_{l,m'-1}^{(1)}) \times (\mu_{lm'}^- \varphi_{l,m'+1}^{(2)*} - \mu_{lm'}^+ \varphi_{l,m'-1}^{(2)*}) \right]. \quad (60)$$

Based on the result that  $\varphi_{lm'}$  decays exponentially with  $m'$ , we may disregard the sum over  $m'$  for the purpose of finding the scaling with  $l_{\max}$ . We then obtain the estimate

$$\Delta S_{00}^{l_{\max}} \sim \partial_r \varphi_{l_{\max}0'}^{(1)} \partial_r \varphi_{l_{\max}0'}^{(2)} + l_{\max}^2 \varphi_{l_{\max}0'}^{(1)} \varphi_{l_{\max}0'}^{(2)}. \quad (61)$$

Note that the  $t$  derivatives in the original source simply contribute to the second term here. They appear in Eq. (60) as the term proportional to  $\Omega^2$ , the dominant piece of which is given by  $\frac{1}{2}\Omega^2 l(l+1) \varphi_{l0'}^{(1)} \varphi_{l0'}^{(2)}$ .

We now appeal to standard results for the large- $l$  behavior of  $\varphi_{l0'}^{\mathcal{P}}$  and  $\varphi_{l0'}^{\mathcal{R}}$  [37]. It is well known that when evaluated on the particle, (a)  $\partial_r^n \varphi_{l0'}^{\mathcal{P}} Y_{l0'} \sim l^n$  and  $\partial_r^n \varphi_{l0'}^{\mathcal{R}} Y_{l0'} \sim l^{n-k}$  for a  $k$ th-order puncture, and (b) the odd negative powers of  $l$  in  $\partial_r^n \varphi_{l0'}^{\mathcal{R}} Y_{l0'}$  identically vanish. Noting that  $Y_{l0'}(0, \beta) \sim l^{1/2}$ , we infer that  $\varphi_{l0'}^{\mathcal{P}} \sim l^{-1/2}$ ,  $\partial_r \varphi_{l0'}^{\mathcal{P}} \sim l^{1/2}$ ,  $\varphi_{l0'}^{\mathcal{R}} \sim l^{-5/2-2\lfloor \frac{k-1}{2} \rfloor}$ , and  $\partial_r \varphi_{l0'}^{\mathcal{R}} \sim l^{-1/2-2\lfloor \frac{k}{2} \rfloor}$ , where  $\lfloor s \rfloor$  denotes the largest integer less than or equal to  $s$ . These results hold at  $\Delta r = 0$ ; at finite  $\Delta r$ , they transition into exponential decay in the now familiar manner. Substituting this behavior into Eq. (61) yields

$$\Delta S_{00}^{l_{\max}}[\varphi^{\mathcal{R}}, \varphi^{\mathcal{R}}] \sim l_{\max}^{-1-4\lfloor \frac{k}{2} \rfloor} + l_{\max}^{-3-4\lfloor \frac{k-1}{2} \rfloor} \quad (62a)$$

$$\sim l_{\max}^{1-2k} \quad (62b)$$

and

$$\Delta S_{00}^{l_{\max}}[\varphi^{\mathcal{R}}, \varphi^{\mathcal{P}}] \sim l_{\max}^{-2\lfloor \frac{k}{2} \rfloor} + l_{\max}^{-1-2\lfloor \frac{k-1}{2} \rfloor} \quad (63a)$$

$$\sim l_{\max}^{1-k}. \quad (63b)$$

In Eqs. (62a) and (63a), the first term arises from  $(\partial_r \varphi)^2$  and the second arises from  $(\partial_t \varphi)^2 + \frac{1}{r^2} \partial_A \varphi \partial^A \varphi$ ; these two terms alternate in dominance from one  $k$  to the next.

To extend our estimates to generic  $lm$  modes, we note that in Eq. (32), when  $l_1 \sim l_{\max} \gg l$ , the triangle inequality also enforces  $l_2 \sim l_{\max} \gg l$ . We can then appeal to the approximation

$$\begin{pmatrix} l & l_1 & l_2 \\ m & m_1 & m_2 \end{pmatrix} \approx (-1)^{l_2+m_2} \frac{d_{m,l_2-l_1}^l(\gamma)}{\sqrt{l_1+l_2+1}} \sim \frac{1}{l_{\max}^{1/2}} \quad (64)$$

for  $l \ll l_1, l_2$ , where  $\cos \gamma = (m_1 - m_2)/(l_1 + l_2 + 1)$ . This implies

$$C_{l_1 m_1 s_1 l_2 m_2 s_2}^{l m s} \sim l_{\max}^0. \quad (65)$$

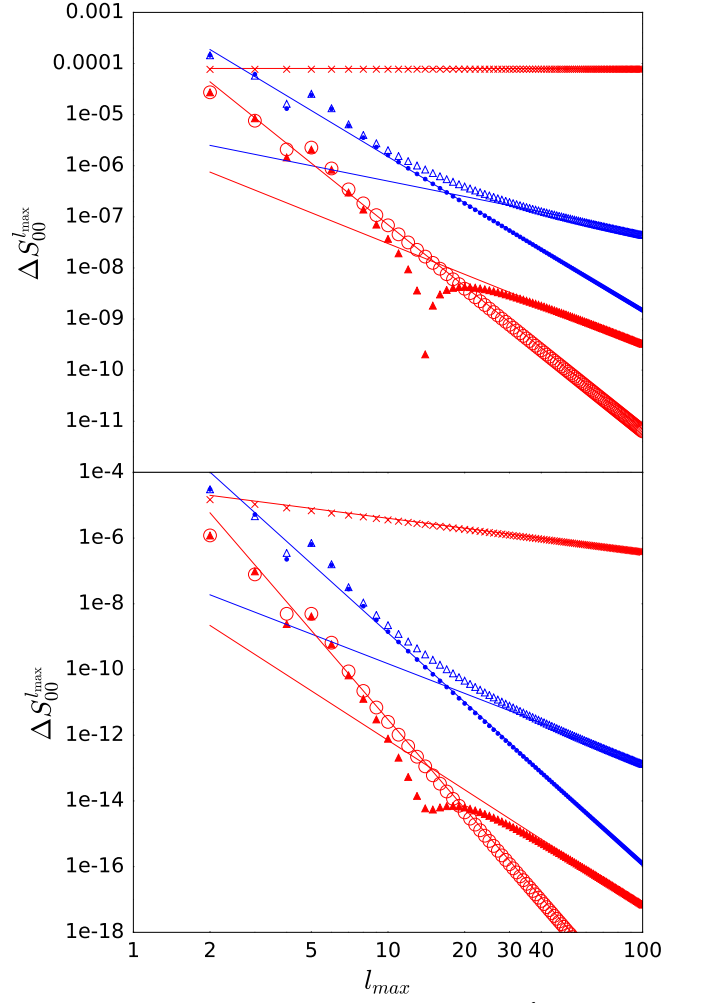


FIG. 6. Comparison of two contributions to  $\Delta S_{00}^{l_{\max}}[\varphi^{\mathcal{R}}, \varphi^{\mathcal{P}}]$  (top panel) and  $\Delta S_{00}^{l_{\max}}[\varphi^{\mathcal{R}}, \varphi^{\mathcal{R}}]$  (bottom), using the same parameters as in Fig. 5. Red symbols represent the contribution from  $\partial_r \varphi^{(1)} \partial_r \varphi^{(2)}$  in Eq. (26), and blue symbols, the contribution from  $\partial_t \varphi^{(1)} \partial_t \varphi^{(2)} + \frac{1}{r^2} \Omega^{AB} \partial_A \varphi^{(1)} \partial_B \varphi^{(2)}$ . For the red symbols, crosses correspond to  $k = 1$ , solid triangles to  $k = 2$  and  $k = 3$ , and open circles to  $k = 4$ ; for the blue symbols, open triangles correspond to  $k = 1$  and  $k = 2$ , and solid circles to  $k = 3$  and  $k = 4$ . The reference lines are proportional to  $l_{\max}^0$ ,  $l_{\max}^{-1}$ ,  $l_{\max}^{-2}$ ,  $l_{\max}^{-3}$ , and  $l_{\max}^{-4}$  in the top panel, and to  $l_{\max}^{-1}$ ,  $l_{\max}^{-3}$ ,  $l_{\max}^{-5}$ ,  $l_{\max}^{-7}$ , and  $l_{\max}^{-9}$  in the bottom panel. For  $k = 1$ , the dominant contribution comes from the red crosses; for  $k = 2$ , the open blue triangles; for  $k = 4$ , the solid blue circles. For  $k = 3$ , the dominant contribution appears to come from the solid blue circles, but because the solid red triangles are falling more slowly, they will eventually become dominant at sufficiently large  $l_{\max}$ .

Given this, we can apply the same arguments as above and find the same scaling estimates:  $\Delta S_{lm}^{l_{\max}}[\varphi^{\mathcal{R}}, \varphi^{\mathcal{R}}] \sim l_{\max}^{1-2k}$  and  $\Delta S_{lm}^{l_{\max}}[\varphi^{\mathcal{R}}, \varphi^{\mathcal{P}}] \sim l_{\max}^{1-k}$ . From this, we again conclude that at least a third-order puncture is needed to ensure convergence.

We now return to the numerically determined scalings in Eqs. (57) and (58). Comparing them to Eqs. (62b) and

(63b), we see that the numerical estimates agree with the analytical ones except in the case of  $k = 3$ , as mentioned previously. This discrepancy stems from Eqs. (62a) and (63a). There we see that for a given  $k$ , two power laws compete for dominance. In practice, we find that the coefficients of these power laws can dramatically differ. Let us focus on  $\Delta S_{00}^{l_{\max}}[\varphi^{\mathcal{R}}, \varphi^{\mathcal{R}}]$  for concreteness. For  $k = 3$ , the dominant power in Eq. (62a) is  $l_{\max}^{-5}$ , and it arises from  $(\partial_r \varphi)^2$ ; the subdominant power is  $l_{\max}^{-7}$ , and it arises from  $(\partial_t \varphi)^2 + \frac{1}{r^2} \partial_A \varphi \partial^A \varphi$ . In our numerical results, we only see the latter, subdominant behavior. Why? Because it comes with an enormously larger numerical coefficient. This is demonstrated in Fig. 6, which plots the contributions from  $(\partial_r \varphi)^2$  and  $(\partial_t \varphi)^2 + \frac{1}{r^2} \partial_A \varphi \partial^A \varphi$  separately. Each of the separate terms is in agreement with Eqs. (62a) and (63a), but we see that for  $k = 3$ ,  $\Delta[(\partial_r \varphi)^2]_{00}^{l_{\max}}$  is hugely suppressed relative to  $\Delta[(\partial_t \varphi)^2 + \frac{1}{r^2} \partial_A \varphi \partial^A \varphi]_{00}^{l_{\max}}$ , even though  $\Delta[(\partial_r \varphi)^2]_{00}^{l_{\max}}$  is decaying more slowly. In fact, by fitting the curves, we can estimate that for  $k = 3$  and  $r_0 = 10$ , the true asymptotic behavior would only become numerically apparent at  $l_{\max} > 450$ .

This competition between terms appears to be a robust feature of the model: numerical investigations show that it is independent of  $l$  and  $m$  and largely independent of  $r_0$ , though it subsides at smaller values of  $r_0$ . Furthermore, the underlying cause is not confined to  $k = 3$ , as we find that the coefficients of various powers of  $1/l_{\max}$  in  $\Delta S_{lm}^{l_{\max}}$  often differ by factors of  $10^4$  or more. Indeed, this is true not just in  $\Delta S_{lm}^{l_{\max}}$ , but also within the individual contributions  $\Delta[(\partial_r \varphi)^2]_{lm}^{l_{\max}}$ ,  $\Delta[(\partial_t \varphi)^2]_{lm}^{l_{\max}}$ , and  $\frac{1}{r^2} \Delta[\partial_A \varphi \partial^A \varphi]_{lm}^{l_{\max}}$ . We have no reason to believe that this is particular to our model. Wildly disparate coefficients of the powers of  $1/l_{\max}$  could very well occur in the gravitational case as well. Because of this, in principle, one might encounter a situation in which one's numerical results had *appeared* to converge, when in fact a divergent power of  $1/l_{\max}$  was still waiting to emerge at larger  $l_{\max}$ . One can only eliminate this possibility by appealing to analytical estimates of the sort in Eqs. (62b) and (63b).

With this additional impetus, we now extend our estimates to the gravitational case. Because  $\delta^2 G_{ilm}$  has the same form as  $S_{lm}$ , and because  $h_{ilm}^{\mathcal{R}}$  and  $h_{ilm}^{\mathcal{P}}$  have the same behavior as  $\varphi_{lm}^{\mathcal{P}}$  and  $\varphi_{lm}^{\mathcal{R}}$ , similar estimates will apply. The only difference between the two cases is that  $\delta^2 G$  contains terms of the form  $h \partial^2 h$  and terms that mix  $t, r, \theta^A$  derivatives. Assume we can account for these changes by adopting a generic form

$$\begin{aligned} \Delta \delta^2 G_{ilm}^{l_{\max}} &\sim \partial_r h_{jl_{\max}0'} \partial_r h_{kl_{\max}0'} + l_{\max}^2 h_{jl_{\max}0'} h_{kl_{\max}0'} \\ &\quad + l_{\max} h_{jl_{\max}0'} \partial_r h_{kl_{\max}0'} \\ &\quad + h_{jl_{\max}0'} \partial_r^2 h_{kl_{\max}0'} \end{aligned} \quad (66)$$

in place of Eq. (61). Using  $\partial_r^2 h_{il0'}^{\mathcal{P}} \sim l^{3/2}$ ,  $\partial_r^2 h_{il0'}^{\mathcal{R}} \sim l^{1/2}$  for  $k = 1$ ,  $\partial_r^2 h_{il0'}^{\mathcal{R}} \sim l^{-1/2-2\lfloor \frac{k-1}{2} \rfloor}$  for  $k > 1$ , and the scalings given above for the lower derivatives, we find that  $\Delta \delta^2 G_{ilm}^{l_{\max}}[h^{\mathcal{R}}, h^{\mathcal{P}}] \sim l_{\max}^{1-k}$  and  $\Delta \delta^2 G_{ilm}^{l_{\max}}[h^{\mathcal{R}}, h^{\mathcal{R}}] \sim$

$l_{\max}^{-k-2\lfloor \frac{k-1}{2} \rfloor}$ . The first of these convergence rates is the slower of the two, and it is identical to the scalar model. Therefore, we conclude that like in the scalar model, for our strategy to be effective in the gravitational case, *it requires at least a third-order puncture  $h_{\mu\nu}^{1\mathcal{P}}$ .*

## V. COMPUTING $S_{lm}[\varphi^{\mathcal{P}}, \varphi^{\mathcal{P}}]$

The only term that remains to be computed in Eq. (10) is  $S_{lm}[\varphi^{\mathcal{P}}, \varphi^{\mathcal{P}}]$ . As we described in the outline of our strategy, we calculate the modes of  $S_{lm}[\varphi^{\mathcal{P}}, \varphi^{\mathcal{P}}]$  by substituting the 4D expression (40) into the 4D expression for  $S$  and then integrating against spherical harmonics to obtain the modes.

More precisely, our procedure is summarized by the following four steps:

1. Begin with the puncture field (40) in the rotated coordinates  $\alpha^{A'}$ .
2. Construct the 4D expression  $S[\varphi^{\mathcal{P}}, \varphi^{\mathcal{P}}]$  in  $\alpha^{A'}$  coordinates using Eq. (33).
3. Decompose  $S[\varphi^{\mathcal{P}}, \varphi^{\mathcal{P}}]$  into  $lm'$  modes  $S_{lm'}[\varphi^{\mathcal{P}}, \varphi^{\mathcal{P}}]$  by evaluating the integrals (34).
4. Use Eq. (39) to obtain the  $lm$  modes  $S_{lm}[\varphi^{\mathcal{P}}, \varphi^{\mathcal{P}}]$ .

The nontrivial step in this procedure is the evaluation of the integrals (34). We perform that evaluation in the same manner as we did the integrals in Sec. IV B. Again we use two independent methods of evaluation: fully numerical and mixed analytical-numerical. The only new features of the integrals is that the integrand now contains explicit factors of  $\sin \alpha$  and  $\cos \alpha$  as well as higher powers, and even powers, of  $\rho$  in their denominator. Because Eq. (44) is defined only for odd  $n$ , the method described in Sec. IV B 1 is not immediately applicable; an even- $n$  analog of Eq. (44) would be required. However, the even powers of  $n$  are readily handled by the methods described in Secs. IV B 2 and IV B 4.

After performing the integrals, we arrive at our promised result displayed in Fig. 2. There we see that near the particle, where  $S_{lm}[\varphi^{\text{ret}}, \varphi^{\text{ret}}]$  converges too slowly with  $l_{\max}$  to see any singularity at  $\Delta r = 0$ , our computed  $S_{lm}$  correctly behaves as  $1/(\Delta r)^2$ . Further from the particle, where  $S_{lm}[\varphi^{\text{ret}}, \varphi^{\text{ret}}]$  rapidly converges with  $l_{\max}$ , our computed  $S_{lm}$  correctly recovers  $S_{lm}[\varphi^{\text{ret}}, \varphi^{\text{ret}}]$ .

## VI. CONCLUSION

We have now demonstrated that our strategy successfully circumvents the problem of slow convergence described in the introduction. This success is encapsulated by Fig. 2.

The core tools in our strategy are adopted from mode-sum regularization and effective-source schemes, but our

analysis has highlighted several unforeseen complications in applying these standard methods. Specifically, we have found that notable intricacies arise in computing mode decompositions in rotated coordinates that place the particle at the north pole. Traditionally, the time dependence of the rotation could be treated cavalierly, but in the calculations described here, it must be handled with care; traditionally, only one azimuthal mode (or a specific few [31, 32]) are required in the rotated coordinates, but here a significant number must be computed; and traditionally, the relevant Legendre integrals can often be simplified by analyzing them in the limit  $r \rightarrow r_0$ , but here they must be evaluated *exactly* in some finite range of  $r$  around  $r_0$ .

Although our implementation has been in a simple scalar toy model, our strategy and computational tools are not in any way specific to that model, and they can be applied directly to the physically relevant gravitational problem. For example, for a particle in a Schwarzschild background, the steps involved in that calculation are as follows:

1. Begin with two ingredients:
  - (a) numerically computed tensor-harmonic modes  $h_{ilm}^1$  of the first-order retarded field in the unrotated coordinates  $(t, r, \theta^A)$ ,
  - (b) a 4D expression for the puncture  $h_{\mu\nu}^{1\mathcal{P}}$  in the rotated coordinates  $(t, r, \alpha^A)$ .

For a given numerical accuracy target, the higher the order of the puncture, the fewer modes  $h_{ilm}^1$  are required; correspondingly, the more modes of  $h_{ilm}^1$  are computed, the lower the necessary order of the puncture. However, following the discussion in Sec. IV C, the puncture must be of at least third order (counting the leading, one-over-distance term as first order).

2. Using the coupling formula (6), given explicitly in Ref. [30], compute the modes  $\delta^2 G_{ilm}[h^1, h^1]$ . They should be computed over the entire numerical domain except in a region  $\mathcal{R} = [r_0 - a, r_0 + b]$  around the particle, choosing  $\mathcal{R}$  such that it contains all points at which the sums in Eq. (6) fail to numerically converge.
3. In the region  $\mathcal{R}$ , compute the tensor-harmonic modes  $h_{ilm'}^{1\mathcal{P}}$  in the rotated system and then use Wigner D matrices to obtain the modes  $h_{ilm}^{1\mathcal{P}}$  in the unrotated system, as described in Sec. IV B. From the result, compute the modes  $h_{ilm}^{1\mathcal{R}} = h_{ilm}^1 - h_{ilm}^{1\mathcal{P}}$  of the residual field.
4. Using the coupling formula (6), compute the modes  $\delta^2 G_{ilm}[h^{1\mathcal{P}}, h^{1\mathcal{R}}]$  and  $\delta^2 G_{ilm}[h^{1\mathcal{R}}, h^{1\mathcal{R}}]$  in  $\mathcal{R}$ .
5. Following the treatment of time derivatives in the Appendix, express  $\delta^2 G_{\mu\nu}[h^{1\mathcal{P}}, h^{1\mathcal{P}}]$  in the rotated coordinates  $(t, r, \alpha^A)$ . In  $\mathcal{R}$ , compute the modes

$\delta^2 G_{ilm}[h^{1\mathcal{P}}, h^{1\mathcal{P}}]$  in the same manner that one computed  $h_{ilm}^{1\mathcal{P}}$ .

6. Sum the results  $\delta^2 G_{ilm}[h^{1\mathcal{P}}, h^{1\mathcal{P}}] + 2\delta^2 G_{ilm}[h^{1\mathcal{P}}, h^{1\mathcal{R}}] + \delta^2 G_{ilm}[h^{1\mathcal{R}}, h^{1\mathcal{R}}]$  to obtain the complete  $\delta^2 G_{ilm}$  in the region  $\mathcal{R}$ . Combined with the result from step 2, this provides  $\delta^2 G_{ilm}$  everywhere in the numerical domain.

This general procedure would also apply to any other nonlinear perturbative problem containing localized singularities, so long as (i) one wished to decompose the problem into harmonics (or some set of orthogonal polynomials) and (ii) one had access to a local, non-decomposed approximation to the singularity.

We recently reported [36] how the strategy presented here has been combined with those developed in Refs. [29, 31, 32] to compute second-order self-force effects on quasi-circular orbits in Schwarzschild spacetime. A future paper will describe that calculation in detail.

## ACKNOWLEDGMENTS

We thank Leor Barack and Niels Warburton for helpful discussions. J.M. and A.P. acknowledge support from the European Research Council under the European Union's Seventh Framework Programme (FP7/2007-2013)/ERC Grant No. 304978. B.W. was supported by the Irish Research Council, which is funded under the National Development Plan for Ireland. This material is based upon work supported by the National Science Foundation under Grant Number 1417132.

## Appendix A: Rotations

In Sec. V, we require a 4D representation of  $S = t^{\mu\nu} \partial_\mu \varphi_1^{\mathcal{P}} \partial_\nu \varphi_1^{\mathcal{P}}$ , given only the expression (23) for  $\varphi_1^{\mathcal{P}}$ , an expression written in a coordinate system in which the particle is instantaneously at the north pole. This is nontrivial because there is no explicit time dependence in Eq. (23),<sup>2</sup> making it unclear how to evaluate the  $t$  derivatives in  $S$ . Here we consider two ways of tackling this problem: via a time-dependent rotation and via a one-parameter family of rotations. We will refer to the first as the 4D method, the second as the 2D method. To assist the discussion, we split the unrotated coordinates into  $x^\mu = (x^a, \theta^A)$ , where  $x^a = (t, r)$  and  $\theta^A = (\theta, \phi)$ , thereby splitting the manifold into the Cartesian product  $\mathcal{M}^2 \times S^2$ , where  $\mathcal{M}^2$  is the  $x^a$  plane and  $S^2$  is the unit sphere.

---

<sup>2</sup> This fact is specific to circular orbits. For noncircular orbits, even in these rotated coordinates,  $\varphi_1^{\mathcal{P}}$  would depend on time through its dependence on the orbital radius  $r_p(t)$ .



In the first approach, we would use a 4D coordinate transformation  $x^\mu \rightarrow x^{\mu'} = (x^{a'}, \alpha^{A'})$  given by  $x^{a'} = x^a$  and  $\alpha^{A'} = \alpha^{A'}(\theta^A, t)$ , where  $\alpha^{A'} = (\alpha, \beta)$ , such that at each fixed  $t$ , the transformation would be a 2D rotation that placed the particle at the north pole. In this case, all tensors would transform in the usual 4D way, including tensors tangent  $\mathcal{M}^2$ ; the transformation mixes  $\mathcal{M}^2$  with  $S^2$ . For example, for a dual vector  $w_\mu$  we would have  $w_t \rightarrow w_{t'} = w_t + \dot{\theta}^A w_A$ ,  $w_r \rightarrow w_{r'} = w_r$ , and  $w_A \rightarrow w_{A'} = \Omega^{A'} w_A$ , where

$$\dot{\theta}^A := \frac{\partial \theta^A}{\partial t'}, \quad (\text{A1})$$

$$\Omega^{A'} := \frac{\partial \theta^A}{\partial \alpha^{A'}}. \quad (\text{A2})$$

In the coordinates  $x^{\mu'}$ , the particle would be permanently at the north pole, with four-velocity  $u^{a'} = u^a$  and  $u^{A'} = 0$ . [Since the coordinates are singular at the particle's position at the north pole,  $u^{A'}$  is not strictly well defined. But if we introduce local Cartesian coordinates  $x^{i'} = (r_0 \alpha \cos \beta, r_0 \alpha \sin \beta)$ , then we can establish  $u^{i'} = 0$ , allowing us to freely set  $u^{A'} = 0$ .] In this method, all components would be expressed in the primed coordinate system, meaning the only time derivatives appearing in  $S$  would be  $\partial_{t'} \phi_1^P$ . For circular orbits, these derivatives would trivially vanish because  $\phi_1^P$  contains no explicit dependence on  $t'$ ; the  $t$  dependence would be entirely encoded in the transformation law's dependence on  $\dot{\theta}^A$ .

Although the 4D method is practicable, we henceforth adopt the second, 2D method, for reasons described below. In this approach, instead of a 4D coordinate transformation, we consider a different 2D rotation at each instant of  $t$ . We may write this as  $\alpha_t^{A'} = \alpha^{A'}(\theta^A, t)$ . This is superficially the same as the 4D method, but the time at which the rotation is performed is now a parameter of the rotation rather than a coordinate, and for each value of the parameter, we have a different coordinate system; for example, if the rotation is performed at time  $t_0$ , it induces a coordinate system  $(t, r, \alpha_{t_0}^{A'})$ . Because the transformation is restricted to  $S^2$ , tensors tangent to  $\mathcal{M}^2$  transform

as scalars and those tangent to  $S^2$  transform as tensors on  $S^2$ : for the same dual vector  $w_\mu$  mentioned above, we now have  $w_a \rightarrow w_a$  and  $w_A \rightarrow w_{A'} = \Omega^{A'} w_A$ . Unlike in the 4D method, where the particle was permanently at the north pole, here it is only there at the particular instant at which the rotation is performed, with an instantaneous four-velocity  $(u^a, u^{A'}) = (u^a, u^\phi, 0)$  at that time. [As above, this value of  $u^{A'}$  comes from consideration of the locally Cartesian components, which can be established to be  $u^{i'} = (r_0 u^\phi, 0)$ .] Time derivatives in this method are evaluated as derivatives with respect to the parameter  $t$ :  $\partial_t \phi_1^P = \dot{\alpha}^{A'} \partial_{A'} \phi_1^P$ , where

$$\dot{\alpha}^{A'} := \frac{\partial \alpha^{A'}}{\partial t} = -\Omega^{A'} \dot{\theta}^A. \quad (\text{A3})$$

Here  $\Omega^{A'} := \frac{\partial \theta^A}{\partial \alpha^{A'}} = (\Omega^{A'})^{-1} = \Omega^{A'B'} \Omega_{AB} \Omega_{B'}$ , and the second equality in Eq. (A3) follows from the implicit function theorem.

In our toy model, the above two methods both lead to the result

$$S = (\partial_r \varphi^P)^2 + (r^{-2} \Omega^{A'B'} + \dot{\alpha}^{A'} \dot{\alpha}^{B'}) \partial_{A'} \varphi^P \partial_{B'} \varphi^P. \quad (\text{A4})$$

However, in gravity the two methods would lead to quite different calculations when performing decompositions into tensor harmonics. Furthermore, only the 2D method is immediately applicable to the decomposition strategy of Ref. [32].<sup>3</sup> Hence, the 2D method is preferred here.

All of the above is fairly general. When we specialize to our particular case of circular orbits with frequency  $\Omega$ , the transformation is given by

$$\theta = \arccos(\sin \alpha \sin \beta), \quad (\text{A5})$$

$$\phi = \arccos\{\cos \alpha / \sin[\arccos(\sin \alpha \sin \beta)]\} + \Omega t, \quad (\text{A6})$$

which implies  $(u^a, u^{A'}) = u^t(1, 0, \Omega, 0)$  and

$$\dot{\theta}^A = (0, \Omega), \quad (\text{A7})$$

$$\dot{\alpha}^{A'} = \Omega(-\cos \beta, \cot \alpha \sin \beta). \quad (\text{A8})$$

The final expression for  $S$ , used in our computations in Sec. V, is given by Eq. (A4) with Eq. (A8).

<sup>3</sup> To see this, consider  $\delta^2 G_{\mu\nu}[h^{1P}, h^{1P}]$ . In the strategy used in Ref. [32], as in our 2D method described here, a quantity such as  $\delta^2 G_{tt}$  is treated as a scalar, that scalar is then written in terms of the coordinates  $\alpha^{A'}$ , and it is decomposed into scalar harmonics by integrating against  $Y_{lm}(\alpha^{A'})$ . Contrary to this, in the 4D method, the scalar-harmonic decomposition of  $\delta^2 G_{tt}$  would be constructed from the scalar, vector, and tensor-harmonic decompositions of  $\delta^2 G_{t't'}$ ,  $\delta^2 G_{t'A'}$ , and  $\delta^2 G_{A'B'}$ , using the transformation  $\delta^2 G_{tt} = \delta^2 G_{t't'} + 2\dot{\alpha}^{A'} \delta^2 G_{t'A'} + \dot{\alpha}^{A'} \dot{\alpha}^{B'} \delta^2 G_{A'B'}$ .

- 
- [1] E. Poisson, A. Pound, and I. Vega, Living Rev. Relativity **14**, 7 (2011).  
 [2] A. Pound, "Motion of small bodies in curved spacetimes: an introduction to gravitational self-force," in *Equations of Motion in Relativistic Gravity*, Fundamental Theories of Physics, Vol. 179, edited by D. Puetzfeld, C. Lammerzahl, and B. Schutz (Springer, 2015) arXiv:1506.06245 [gr-qc].  
 [3] A. I. Harte, "Motion in classical field theories and the foundations of the self-force problem," in *Equations of Motion in Relativistic Gravity*, Fundamental Theories of Physics, Vol. 179, edited by D. Puetzfeld, C. Lam-

- merzähl, and B. Schutz (Springer, 2015) arXiv:1405.5077 [gr-qc].
- [4] L. Barack, *Class. Quant. Grav.* **26**, 213001 (2009), arXiv:0908.1664 [gr-qc].
- [5] P. Amaro-Seoane, J. R. Gair, A. Pound, S. A. Hughes, and C. F. Sopuerta, *J. Phys. Conf. Ser.* **610**, 012002 (2015), arXiv:1410.0958 [astro-ph.CO].
- [6] L. Blanchet, S. L. Detweiler, A. Le Tiec, and B. F. Whiting, *Phys. Rev. D* **81**, 084033 (2010), arXiv:1002.0726 [gr-qc].
- [7] S. Akcay, L. Barack, T. Damour, and N. Sago, *Phys. Rev. D* **86**, 104041 (2012), arXiv:1209.0964 [gr-qc].
- [8] L. Blanchet, G. Faye, and B. F. Whiting, *Phys. Rev. D* **90**, 044017 (2014), arXiv:1405.5151 [gr-qc].
- [9] A. Le Tiec, *Int. J. Mod. Phys. D* **23**, 1430022 (2014), arXiv:1408.5505 [gr-qc].
- [10] S. Bernuzzi, A. Nagar, T. Dietrich, and T. Damour, *Phys.Rev.Lett.* **114**, 161103 (2015), arXiv:1412.4553 [gr-qc].
- [11] T. Damour, P. Jaranowski, and G. Schfer, *Phys. Rev. D* **93**, 084014 (2016), arXiv:1601.01283 [gr-qc].
- [12] B. Wardell, “Self-force: Computational strategies,” in *Equations of Motion in Relativistic Gravity*, Fundamental Theories of Physics, Vol. 179, edited by D. Puetzfeld, C. Lammerzahl, and B. Schutz (Springer, 2015) arXiv:1501.07322 [gr-qc].
- [13] M. Colleoni, L. Barack, A. G. Shah, and M. van de Meent, *Phys. Rev. D* **92**, 084044 (2015), arXiv:1508.04031 [gr-qc].
- [14] D. Bini, T. Damour, and A. Gerialico, *Phys. Rev. D* **93**, 064023 (2016), arXiv:1511.04533 [gr-qc].
- [15] T. Osburn, N. Warburton, and C. R. Evans, *Phys. Rev. D* **93**, 064024 (2016), arXiv:1511.01498 [gr-qc].
- [16] S. Hopper, C. Kavanagh, and A. C. Ottewill, *Phys. Rev. D* **93**, 044010 (2016), arXiv:1512.01556 [gr-qc].
- [17] C. Kavanagh, A. C. Ottewill, and B. Wardell, *Phys. Rev. D* **93**, 124038 (2016), arXiv:1601.03394 [gr-qc].
- [18] M. van de Meent, (2016), arXiv:1606.06297 [gr-qc].
- [19] S. Akcay, D. Dempsey, and S. Dolan, (2016), arXiv:1608.04811 [gr-qc].
- [20] T. Hinderer and E. E. Flanagan, *Phys. Rev. D* **78**, 064028 (2008).
- [21] E. Rosenthal, *Phys. Rev. D* **73**, 044034 (2006).
- [22] E. Rosenthal, *Phys. Rev. D* **74**, 084018 (2006).
- [23] S. Detweiler, *Phys. Rev. D* **85**, 044048 (2012), arXiv:1107.2098 [gr-qc].
- [24] A. Pound, *Phys. Rev. Lett.* **109**, 051101 (2012), arXiv:1201.5089 [gr-qc].
- [25] S. E. Gralla, *Phys. Rev. D* **85**, 124011 (2012), arXiv:1203.3189 [gr-qc].
- [26] A. Pound, *Phys. Rev. D* **86**, 084019 (2012), arXiv:1206.6538 [gr-qc].
- [27] A. Pound and J. Miller, *Phys. Rev. D* **89**, 104020 (2014), arXiv:1403.1843 [gr-qc].
- [28] A. Pound, *Phys. Rev. D* **92**, 044021 (2015), arXiv:1506.02894 [gr-qc].
- [29] A. Pound, *Phys. Rev. D* **92**, 104047 (2015), arXiv:1510.05172 [gr-qc].
- [30] A. Pound, “Tensor-harmonic decomposition of the second-order einstein equation in schwarzschild space-time,” (2016), in preparation.
- [31] N. Warburton and B. Wardell, *Phys. Rev. D* **89**, 044046 (2014), arXiv:1311.3104 [gr-qc].
- [32] B. Wardell and N. Warburton, *Phys. Rev. D* **92**, 084019 (2015), arXiv:1505.07841 [gr-qc].
- [33] L. Barack and C. O. Lousto, *Phys. Rev. D* **72**, 104026 (2005), arXiv:gr-qc/0510019 [gr-qc].
- [34] L. Barack and N. Sago, *Phys. Rev. D* **75**, 064021 (2007), arXiv:gr-qc/0701069 [gr-qc].
- [35] S. L. Detweiler and B. F. Whiting, *Phys. Rev. D* **67**, 024025 (2003).
- [36] A. Pound, “Second-order self-force: a progress report,” Talk given at GR21, Columbia University, New York, USA, July 2016. Slides available at [http://www.gr21.org/files/Adam.Pound-Pound\\_\(1\).pdf.gz](http://www.gr21.org/files/Adam.Pound-Pound_(1).pdf.gz).
- [37] A. Heffernan, A. Ottewill, and B. Wardell, *Phys. Rev. D* **86**, 104023 (2012), arXiv:1204.0794 [gr-qc].
- [38] R. Haas and E. Poisson, *Phys. Rev. D* **74**, 044009 (2006), arXiv:gr-qc/0605077 [gr-qc].
- [39] S. Orszag, *Monthly Weather Review* **102**, 56 (1974).
- [40] G. Lohöfer, *Journal of Approximation Theory* **95**, 178 (1998).